TROPESS/CrIS carbon monoxide profile validation with NOAA GML and ATom in situ aircraft observations

Helen M. Worden[1], Gene L. Francis[1], Susan S. Kulawik[2], Kevin W. Bowman[3], Karen Cady-Pereira[4], Dejian Fu[3], Jennifer D. Hegarty[4], Valentin Kantchev[3], Ming Luo[3], Vivienne H. Payne[3], John R. Worden[3], Róisín Commane[5], Kathryn McKain[6,7]

[1]Atmospheric Chemistry Observations and Modeling (ACOM), National Center for Atmospheric Research (NCAR), Boulder, CO, USA
[2]BAER Institute, 625 2nd Street, Suite 209, Petaluma, CA, USA
[3]Jet Propulsion Laboratory / California Institute for Technology, Pasadena, CA, USA
[4]Atmospheric and Environmental Research Inc., Lexington, MA, USA
[5]Dept. of Earth and Environmental Sciences, Lamont-Doherty Earth Observatory, Columbia University, Palisades, NY, USA
[6]Cooperative Institute for Research in Environmental Sciences (CIRES), University of Colorado, Boulder, CO, USA
[7]Global Monitoring Division (GMD), National Oceanic and Atmospheric Administration, Boulder, CO, USA

Correspondence to: Helen Worden (hmw@ucar.edu)

Abstract. The new single pixel TROPESS (TRopospheric Ozone and its Precursors from Earth System Sounding) profile retrievals of carbon monoxide (CO) from the Cross-track Infrared Sounder (CrIS) are evaluated using vertical profiles of in situ observations from the National Oceanic and Atmospheric Administration (NOAA) Global Monitoring Laboratory (GML) aircraft program and from the Atmospheric Tomography Mission (ATom) campaigns. The TROPESS optimal estimation retrievals are produced using the MUSES (MUlti-SpEctra, MUlti-SpEcies, MUlti-Sensors) algorithm which has heritage from retrieval algorithms developed for the EOS/Aura Tropospheric Emission Spectrometer (TES). TROPESS products provide retrieval diagnostics and error covariance matrices that propagate instrument noise as well as the uncertainties from sequential retrievals of parameters such as temperature and water vapor that are required to estimate the carbon monoxide profiles. The validation approach used here evaluates biases in column and profile values and the validity of the retrieval error estimates using the mean and variance of the compared satellite and aircraft observations. CrIS-NOAA GML comparisons had biases of 0.6 % for partial column average volume mixing ratios (VMR) and (2.3, 0.9, -4.5) % for VMR at (750, 511, 287) hPa vertical levels, respectively, with standard deviations from 9 % to 14 %. CrIS-ATom comparisons had biases of -0.04 % for partial column and (2.2, 0.5,-3.0) % for (750, 511, 287) hPa vertical levels, respectively, with standard deviations from 6 % to 10 %. The reported observational errors for TROPESS/CrIS CO profiles have the expected behavior with respect to the vertical pattern in standard deviation of the comparisons. These comparison results give us confidence in the use of TROPESS/CrIS CO profiles and error characterization for continuing the multi decadal record of satellite CO observations.

1. Introduction

Carbon monoxide (CO) is a useful tracer of atmospheric pollution with direct emissions from incomplete combustion such as biomass and fossil fuel burning and secondary production from the oxidation of methane (CH_4) and volatile organic compounds (VOC). Atmospheric CO distributions have a seasonal cycle that is mainly driven by photochemical destruction, which allows CO to build up over winter and early spring in higher latitudes. The lifetime of CO, weeks to months, (e.g., Holloway et al., 2000), is long enough to allow observations of pollution plumes and their subsequent long range transport, but short enough to distinguish the plumes against background seasonal distributions (e.g., Edwards et al., 2004, 2006; Hegarty et al., 2009, 2010). As a dominant sink for the hydroxyl radical (OH), CO plays a critical role in atmospheric reactivity (e.g., Lelieveld et al., 2016) and is considered a short-lived climate pollutant (SLCP) because of its impacts to methane lifetime and carbon dioxide and ozone formation (e.g., Myhre et al., 2014; Gaubert et al., 2017).

Global observations of tropospheric CO from satellites started in 2000 with the NASA Earth Observing System (EOS) Measurement of Pollution in the Troposphere (MOPITT) instrument on Terra (Drummond et al., 2010), followed by the EOS Atmospheric Infrared Spectrometer (AIRS, McMillan et al., 2005) on Aqua launched in 2002, the Scanning Imaging Absorption Spectrometer for Atmospheric Chartography (SCIAMACHY, de Laat et al., 2006) on Envisat launched in 2002, the EOS Tropospheric Emission Spectrometer (TES, Beer et al., 2006) on Aura launched in 2004, the Infrared Atmospheric Sounding Interferometer (IASI, Clerbaux et al., 2009) on the MetOp series beginning in 2006, the Cross-track Infrared Sounder (CrIS, Gambacorta et al., 2014) on the Suomi National Polar-orbiting Partnership (SNPP) satellite launched in 2011, and most recently the Joint Polar Satellite System (JPSS) series, TROPOMI on the Sentinel-5 precursor in 2017, (Borsdorff, et al., 2018) and the Fourier Transform Spectrometer (FTS-2) on the Greenhouse gases Observing SATellite-2 (GOSAT-2, Suto et al., 2021), launched in 2018. Satellite CO observations are assimilated for reanalyses and operational air quality forecasting (e.g., Gaubert, 2016; Inness et al., 2019; Miyazaki et al., 2020) and have been used in inverse modelling analyses to estimate emissions and attribute sources for co-emitted species such as CO_2 (e.g., Kopacz et al., 2010; Jiang et al 2017; Liu et al., 2017; Zheng et al., 2019; Gaubert et al., 2020; Byrne et al., 2021; Qu et al., 2022). Trend analyses of satellite CO observations (e.g. Worden et al., 2013; Buchholz et al., 2021) show a general decline of atmospheric CO over the satellite record globally and in most regions, but with a slowing of this decrease in recent years that emphasizes the need for continued satellite CO observations that are validated and have reliable error characterization.

In this study, we evaluate the biases and reported uncertainties of single field of view (FOV) CO retrievals, from the Cross-track Infrared Sounder (CrIS) onboard the SNPP satellite launched in October, 2011. CrIS is a Fourier Transform Spectrometer (FTS) that has continuation instruments on the current and planned JPSS series with JPSS1/NOAA-20 launched in 2017 and planned launches in 2022, 2028 and 2032 (jpss.noaa.gov). The CrIS CO retrievals evaluated here use the MUSES (MUlti-SpEctra, MUlti-SpEcies, MUlti-Sensors) algorithm (Fu et al., 2016, 2018, 2019) and are processed with the TROPESS (TRopospheric Ozone and its Precursors from Earth System Sounding) Science Data Processing System (Bowman et al., 2021). TROPESS is a NASA project that provides a framework for consistent data processing of ozone and ozone precursors across different satellite instruments. TROPESS retrievals use single FOV radiances in sequential optimal estimation retrievals (Rodgers, 2000) of temperature, water vapor, effective cloud parameters, ozone, CO and other trace gases, allowing for full characterization of the vertical retrieval sensitivity with an averaging kernel and error covariance (Bowman et al., 2006). TROPESS/CrIS CO products differ from other available CrIS CO data products that combine 9 FOVs to obtain a single cloud-cleared radiance and corresponding retrieval of atmospheric parameters such as the NOAA Unique Combined Atmospheric Processing System (NUCAPS) (Gambacorta et al., 2014, 2017; Nalli et al., 2020) and the Community Long-term Infrared Microwave Combined Atmospheric Product System (CLIMCAPS) (Smith and Barnet, 2020).

TROPESS data products report a separate matrix for the observational error terms along with the total retrieval error covariance that includes the contribution of smoothing error. This is important for evaluation of retrieval errors using in situ profiles since the validation comparison removes the effect of smoothing in the retrieval by applying the retrieval averaging kernel and a priori to the in situ profile before differencing (Rodgers and Connor, 2003). Similar comparisons were performed in the recent validation study for the MUSES single FOV CO retrievals from the Aura Atmospheric Infrared Sounder (AIRS) of Hegarty et al. (2022).

Section 2 describes the TROPESS retrievals and CO data products in more detail, and Section 3 describes the validation in situ data from the National Oceanic and Atmospheric Administration (NOAA) Global Monitoring Laboratory (GML) aircraft network and the Atmospheric Tomography Mission (ATom) campaigns. The validation methods are presented in Section 4 and results are shown in Section 5 with a summary and conclusions in Section 6.

2. TROPESS/CrIS single field of view CO profile retrievals

The first Cross-track Infrared Sounder (CrIS) was launched 28 October, 2011 on the SNPP satellite into a sun-synchronous polar orbit with an altitude near 830 km, and an equator-crossing time (ascending node) near 13:30 LT. CrIS is a Fourier Transform Spectrometer (FTS) operating in three spectral bands between 648 cm^{-1} and 2555 cm^{-1}. This includes the R-branch of the thermal infrared (TIR) CO (0-1) fundamental band above 2155 cm^{-1}. After launch, spectral radiance data that included the CO band were collected using a spectral resolution of 2.5 cm^{-1}. This resolution was relatively coarse and significantly limited the vertical sensitivity of CO retrievals (Gambacorta et al., 2014). Following the decision to collect data at full-spectral resolution (δ = 0.625 cm^{-1}), these finer resolution spectral radiances have been available since 4 December 2014. Here we only utilize the full-spectral resolution CrIS data.

2.1 TROPESS retrieval approach

TROPESS data processing (Bowman et al., 2021) produces retrievals of temperature, water vapor and trace gases such as ozone (O_3), methane (CH_4), carbon monoxide (CO), ammonia (NH_3) and peroxyacetyl nitrate (PAN) from single and multiple instruments including AIRS and OMI, CrIS and TROPOMI. The MUSES retrieval algorithm used in TROPESS was developed with heritage from Aura/TES retrieval processing. Bowman et al. (2021) describe the sequential MUSES retrievals of temperature, water vaper and effective cloud properties for each FOV that are necessary for the retrieval of CO. Each step in the sequence includes an iterative retrieval with a forward model and updated estimate of the state vector of atmospheric parameters following the *maximum a posteriori* (MAP) method. The forward model for radiative transfer at

CrIS TIR wavelengths uses Optimal Spectral Sampling (OSS, Moncet et al., 2015), which includes effective cloud optical depth and height parameters (Eldering et al., 2008; Kulawik et al., 2006).

Here we analyze TROPESS/CrIS TIR-only CO retrievals that use the 2181-2200 cm^{-1} spectral range. A priori profiles for TROPESS CO retrievals are taken from the model climatology used in Aura/TES processing (MOZART, Brasseur et al., 1998), with monthly variation over a 30° latitude and 60° longitude grid. The a priori uncertainty covariance matrix used to constrain the retrieval is the same as used for MOPITT profiles (Deeter et al., 2010) with 30 % uncertainty for vertical CO parameters at all levels and correlation lengths corresponding to 100 hPa between them in the troposphere.

The TROPESS CO products have quality flags for screening cases that did not converge or that have unphysical results. This screening checks the magnitude and spectral structure of radiance residuals, cloud retrieval characteristics, and deviation of surface emissivity from a priori values. Specifically, retrievals with good data quality of 1 have: radiance residual standard deviation less than 12 times the radiance error, an absolute value of the radiance residual mean less than 0.7 times the radiance error, KdotDL (the normalized dot product of the Jacobians and the radiance residual) less than 0.8, LdotDL (the normalized dot product of the radiance and the residual) less than 0.6, cloud top pressures below 90 hPa, mean cloud optical depths less than 50, cloud variability (variation with respect to wavenumber) less than 3, and mean surface emissivity that did not change by more than 0.06. These threshold values are based on comparisons with in situ data and other satellite data to determine when retrievals are valid.

2.2 TROPESS/CrIS CO data examples

Figure 1 shows an example of TROPESS/CrIS CO data for 12 September 2020 when there were significant fires in the western US. These retrievals are from a special data collection that processed scenes selected from 0.25° x 0.25° latitude/longitude sub-sampling to enable throughput with the available computing capacity (Bowman et al., 2021). The data in this collection are pre-filtered for quality (see Section 2.1) and Fig. 1a shows all available day and night retrievals. Fig. 1b shows the data after higher cloudy scenes are removed (i.e, cloud tops with pressure < 700 hPa and cloud effective optical depth > 0.1). For reference, Fig. 1c shows the mid-tropospheric average CO volume mixing ratio (VMR) for the a priori profiles used in the retrievals and Fig. 1d shows a NASA Worldview (worldview.earthdata.nasa.gov) image from SNPP/VIIRS (Visible Infrared Imaging Radiometer Suite) with clouds and smoke shown in true color and red areas indicating fire and thermal anomalies. Since vertical profile retrievals using TIR radiances have sensitivity to CO mainly in the free troposphere, Fig. 1 shows individual retrievals with average VMR from vertical layers between 700 to 350 hPa. When all scenes are included, the average degrees of freedom for signal (DFS) is 0.99 for the CrIS CO observations in Fig. 1a, and when cloudy scenes are removed (Fig. 1b) the average DFS is 1.14 for the remaining CrIS observations.

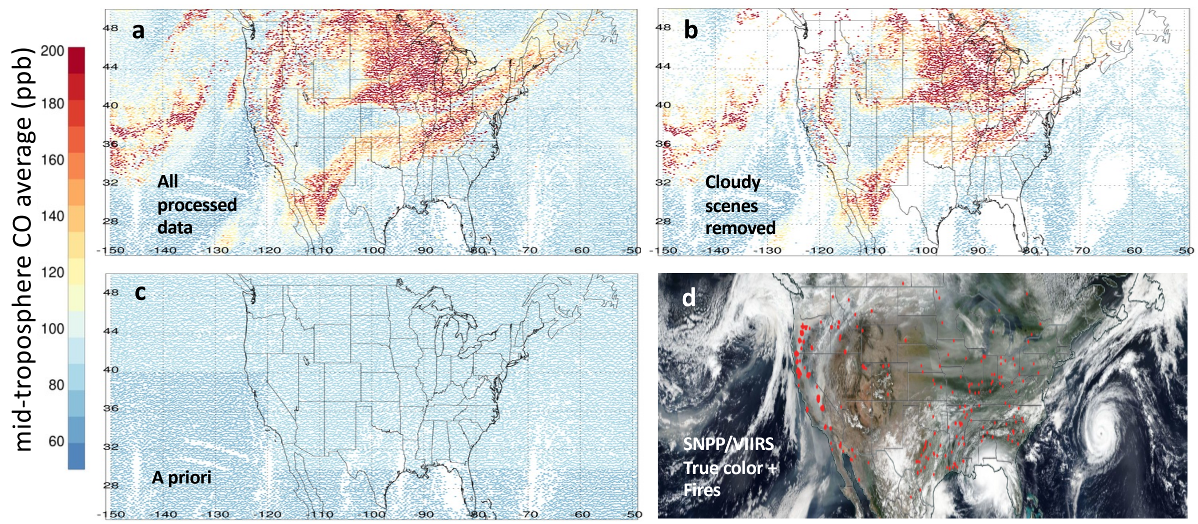

Figure 1. *SNPP TROPESS/CrIS and SNPP/VIIRS observations for 14 September, 2020. Panel (a) shows the average CO VMR for 700 to 350 hPa for all processed TROPESS CO retrievals with good data quality (see text). Panel (b) shows the same free troposphere CO averages as (a) but with cloudy scenes removed (see text). Panel (c) shows the average TROPESS a priori CO VMR for 700 to 350 hPa. Panel (d) shows the NASA Worldview SNPP/VIIRS image for 14 September, 2020 with clouds and smoke (true color) and fire thermal anomalies (red).*

As stated in the introduction, the TROPESS single FOV products are different from the NUCAPS and CLIMCAPS products that combine 9 FOVs in a retrieval from a single cloud-cleared radiance (Susskind et al., 2003). These multiple FOV products have the advantage of increased global coverage in the presence of partially cloudy scenes but with coarser spatial resolution. Figure 2 shows an example of SNPP CLIMCAPS (Barnet, 2019) compared to SNPP TROPESS/CrIS CO products (daytime only) on 13 September 2018 over the Pole Creek Fire in Utah. For CLIMCAPS, trace gas products with less than 1 DFS report mass mixing ratio (MMR) on a single level at the retrieval pressure with peak sensitivity, which is 500 hPa for CO. We converted MMR to VMR for Figure 2. This is compared to the tropospheric column average VMR from TROPESS, so the background VMR values are close, but do not represent the same retrieved quantities. CrIS retrieval center locations are shown by the circles in Fig 2a, 2b, which are not intended to represent the spatial extent of the observations. The CLIMCAPS retrievals show elevated CO from the fire, but these combined FOV retrievals would give an overestimate of the plume width and do not distinguish the larger plume from the smaller fires to the east in Colorado.

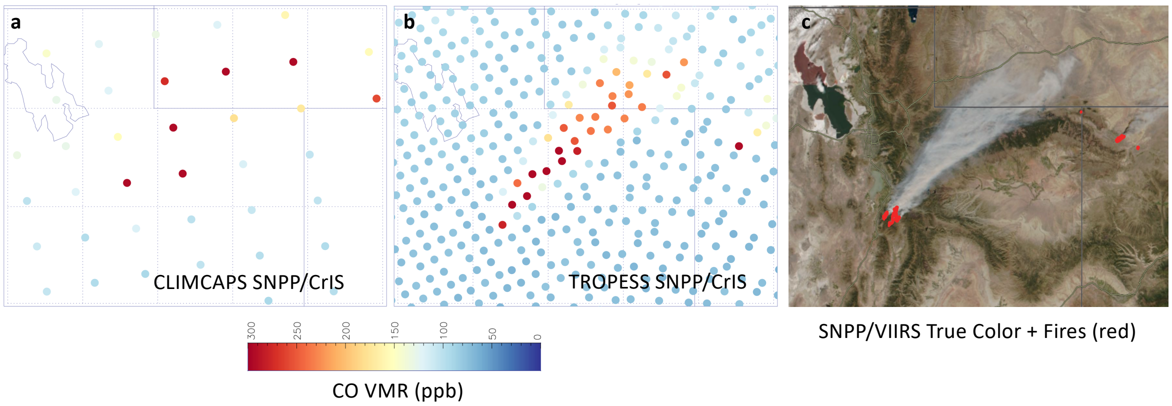

Figure 2. *SNPP Observations of the Pole Creek Fire in Utah, USA, 13 September, 2018. The Great Salt Lake is in the upper left of each panel and state borders with Idaho, Wyoming and Colorado are indicated by solid straight lines. Dotted lines indicate a 1° latitude by 1° longitude grid, with top/left corner at 42°N, -113°E. Panel (a) shows CLIMCAPS/CrIS CO at 500 hPa (MMR converted to VMR). Panel (b) shows the TROPESS/CrIS tropospheric CO column average VMR and panel (c) shows the corresponding NASA Worldview SNPP/VIIRS image with clouds and smoke (true color) and fire thermal anomalies (red).*

We note that retrievals of CO in the presence of smoke are not significantly affected by scattering for infrared observations at wavelengths $\lambda \sim 4.6$ µm, such as in the CrIS CO band. This is because Rayleigh scattering, which decreases by $1/\lambda^4$, is completely negligible and Mie scattering would be significant only for particles larger than $\sim \lambda/\pi = 1.5$ µm, (e.g., Seinfeld and Pandis, 1998), while the size distribution for biomass burning smoke particles peaks around 0.3 µm (e.g., Reid et al., 2005). For the same Pole Creek fire in Fig. 2, Juncosa Calahorrano et al. (2021) showed how SNPP/CrIS single pixel MUSES retrievals of acyl peroxy nitrates, also known as PAN, along with CO, can be used to follow fire plume chemical evolution. After subtracting background amounts, the normalized excess mixing ratios (NEMR) of PAN with respect to CO, computed from the CrIS observations for this plume, were consistent with in situ aircraft observations of smoke plumes from the summer 2018 WE-CAN (Western Wildfire Experiment for Cloud Chemistry, Aerosol Absorption, and Nitrogen) campaign.

3. Aircraft Data

3.1 NOAA GML aircraft network

Spanning 3 decades, NOAA GML aircraft network vertical profile observations are taken on semi-regular flights (~1/month) at fixed sites mostly in North America except for one site in Rarotonga, Cook Islands (Sweeney et al., 2015). These flights collect air samples using an automated flask system to obtain vertical profiles for each trace gas measured, from near the surface to around 400 hPa, depending on aircraft limitations at each site. Flask samples are then sent for laboratory analysis of a multitude of trace gases including CO, which was measured with vacuum UV-fluorescence spectroscopy during the time period of this analysis. CO mixing ratios are reported relative to the WMO X2014A scale (https://gml.noaa.gov/ccl/co_scale.html) and have reproducibility ~1 ppb (Sweeney et al., 2015). NOAA GML aircraft profiles of CO have been used for the long-term validation of the MOPITT CO record, with updated validation for each new data version (Deeter et al., 2019 and references therein). For the current analysis, we use NOAA GML aircraft network observations of CO collected during 2016 and 2017 from 7 locations (Table 1).

3.2 ATom aircraft campaigns

The Atmospheric Tomography Mission (ATom) was designed to study the most remote regions of the Pacific and Atlantic ocean air masses in each season (Thompson et al., 2022), which also makes the data valuable for validating satellite CO observations over a range of latitudes, with mostly background CO concentrations, except for where transported pollution plumes were encountered (Deeter et al., 2019; 2022; Martínez-Alonso et al., 2020; Hegarty et al., 2022). We use CO profiles from the quantum cascade laser spectrometer (QCLS) on the ATom campaigns 1-4 (see Table 1). These NASA DC-8 flights obtained vertical profiles from 0.2 to 12 km altitude (~290 hPa) by ascending or descending approximately every 220 km. CO was measured at 1 Hz with QCLS reproducibility around 0.15 ppbv (McManus et al., 2010, Santoni et al., 2014). The QCLS data were calibrated to the X2014A CO WMO scale maintained by the NOAA GML.

Table 1. Aircraft in situ validation observations used in this study.

NOAA/GML Network flask/UV spectrometer (±1ppb CO)			
Code/Site name	Latitude (°N)	Longitude (°W)	Dates available
RTA/Raratonga	-21.25	159.83	2000-2021
TGC/Offshore Corpus Christi,TX	27.73	96.86	2003-2021
CMA/Offshore Cape May, NJ	38.83	74.32	2005-2022
THD/Trinidad Head, CA	41.05	124.15	2003-2022
NHA/Offshore Portsmouth, NH	42.95	70.63	2003-2022
ESP/Estevan Pt., BC	49.38	128.54	2002-2021
ACG/Alaska Coast Guard	57.74	152.50	2009-2021
NASA/ATom QCLS (±0.15ppb CO)			
ATom 1-4 Pacific	75 to -65	150 to 70	July 2016, Jan. 2017, Sep. 2017, April 2018
ATom 1-4 Atlantic	-75 to 80	65 to 20	Aug. 2016, Feb. 2017, Oct. 2017, May 2018

https://gml.noaa.gov/ccgg/aircraft/
https://espo.nasa.gov/atom/content/ATom

4. Validation Methodology

4.1 Data selection, coincidence criteria and vertical extension of aircraft profiles

TROPESS/CrIS CO profiles are selected for comparison if they have retrieval quality of 1 and effective cloud optical depth less than 0.1 to ensure non-cloudy CrIS observations. We then find all eligible CrIS and aircraft profile pairs within 9 hours and 50 km distance. This has been a standard coincidence distance criterion for several validation studies (e.g., Deeter et al., 2019; 2022; Hegarty et al., 2022). Tang et al. (2020) found very little sensitivity in MOPITT CO validation results for 25, 50, 100 and 200 km coincidence except for the cases with a 25 km radius that resulted in an insufficient number of matches for meaningful statistics. The Tang et al. (2020) study also tested the time coincidence criterion (12, 6, 2 and 1 hour) with similar conclusions. Application of the 9 hour/ 50 km coincidence criteria yielded 2092 CrIS/aircraft profile pairs for NOAA GML flights from 2016 and 2017 and 1052 profile pairs for the ATom 1-4 campaigns. Since the aircraft profiles used for validation do not span the full vertical range of satellite retrieved profiles, we must extend these with a reasonable approximation of atmospheric CO to facilitate the comparison as described below in section 4.2. Here we use the TROPESS a priori profiles (from model climatology, described above) to extend the in situ profiles above the highest altitude sampled. The a priori profile is scaled to match the CO abundance of the aircraft measurement at the highest altitude. The choice of model and approach for extending the aircraft profiles are examined more in Tang et al. (2020) and Hegarty et al. (2022), with similar conclusions that the impacts apply mostly to bias estimates in the middle to upper troposphere. Martínez-Alonso et al. (2022) compute the uncertainty introduced by this extension explicitly using NOAA AirCore in situ balloon profiles that sample into the stratosphere (Karion et al., 2010). This uncertainty is computed for validation using aircraft profiles (with top samples around 400 hPa for NOAA/GML) by comparing MOPITT profiles to truncated and extended AirCore profiles vs. the true full AirCore profiles. The comparison error introduced by the extension was at most 3 % around 300 hPa, and much less than the standard deviation of MOPITT and full AirCore profile differences (~7-10 %) in the upper troposphere. We also note that for ATom profiles, the highest altitude samples are normally taken around 12 km (~200 hPa) and the profile extension therefore has minimal impact on tropospheric validation results.

4.2 Comparison of TROPESS satellite and aircraft observations

In order to account for the satellite observational and retrieval approach, including prior information, when comparing satellite retrieval products to in situ measurements of CO, we apply the instrument operator to convert the in situ profile into the values that would be retrieved for the same air mass assuming the satellite instrument and retrieval (Jones et al., 2003, Rodgers and Conner, 2003, Worden et al., 2007):

$$\hat{x}_{val} = x_a + \mathbf{A}(x_{val} - x_a) \quad (1)$$

where x_{val} is the aircraft or sonde in situ profile being used for validation (following extension, described above, and linear interpolation to the satellite vertical grid), x_a is the a priori profile used in the TROPESS retrieval, **A** is the averaging kernel matrix that describes the observation and retrieval vertical sensitivity to the true state and $\hat{x}_{val}$ is the in situ validation profile transformed by the satellite instrument operator. This operation accounts for both the broad vertical resolution (or "smoothing") of remotely sensed measurements and the influence of the a priori, which is especially important in the vertical ranges where satellite observations have low sensitivity to CO abundance. Figure 3 shows an example of the averaging kernel **A** and a validation comparison where Eq. 1 is applied to an ATom in situ profile.

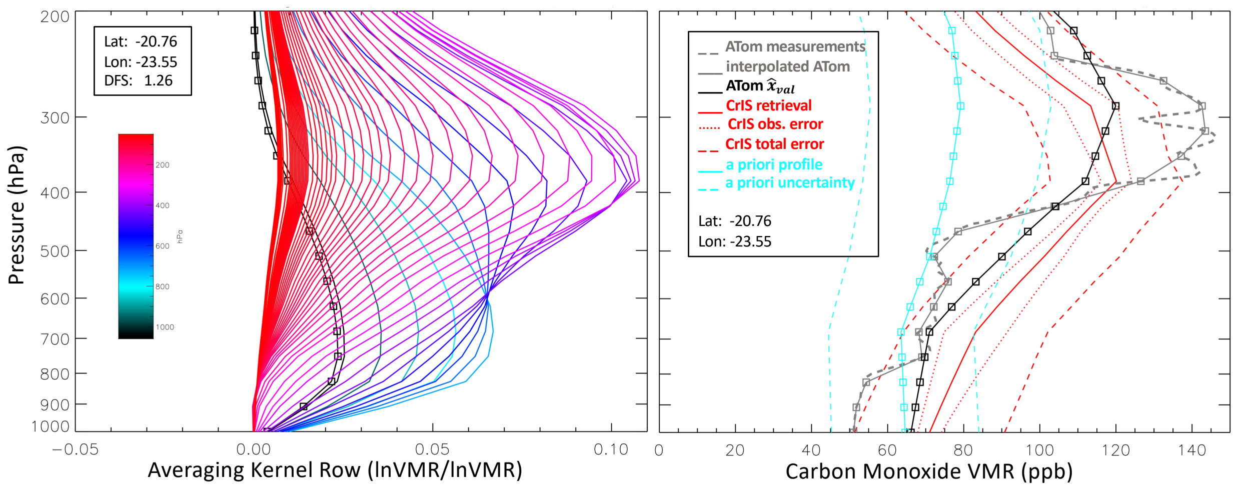

Figure 3. *Examples of TROPESS/CrIS CO averaging kernel (**A**) (left panel) and the validation process (right panel). The colors of the averaging kernel indicate the pressure level (66 levels from 1017.45 to 0.1 hPa) corresponding to each row, with the surface level row also indicated by the squares. The degrees of freedom for signal (DFS), given by the sum of the diagonal (i.e. trace) of this averaging kernel is 1.26. The right panel shows the CrIS CO profile retrieval (solid red line) with total error (dashed red lines), observation error (dotted red lines), apriori profile (solid cyan line with squares) and diagonal uncertainty (dashed cyan lines). The closest ATom aircraft profile had 10.4 km; 3.5 hr coincidence. The original ATom profile (dashed grey line) is interpolated to the CrIS vertical grid (solid grey with squares) and transformed by the instrument operator to give ATom* $\hat{x}_{val}$ *(Eq. 1) (solid black line with squares).*

4.3 Evaluating TROPESS CO reported observational errors

Following Bowman et al., (2006, 2021), for retrieved parameter $\hat{x}$ (e.g., CO abundance) with a priori covariance $\mathbf{S_a}$, radiance measurement covariance $\mathbf{S_e}$, Jacobian matrix $\mathbf{K} = \frac{\partial L}{\partial x}$, for radiance *L(x)*, gain matrix $\mathbf{G} = (\mathbf{K}^T\mathbf{S}_e^{-1}\mathbf{K} + \mathbf{S}_a^{-1})^{-1}\mathbf{K}^T\mathbf{S}_e^{-1}$ and averaging kernel $\mathbf{A} = \mathbf{GK}$, the a posteriori error covariance can be written as the sum of:

$$\mathbf{S}_{\hat{x}} = \boldsymbol{S}_{smoothing} + \mathbf{S}_{observational} \quad (2)$$

with $\mathbf{S}_{smoothing} = (\mathbf{I} - \mathbf{A}_{xx})\mathbf{S}_a(\mathbf{I} - \mathbf{A}_{xx})^{\mathrm{T}}$ and

$$\mathbf{S}_{observational} = \mathbf{S}_{noise} + \mathbf{S}_{cross-state} + \mathbf{S}_{systematic} \quad (3)$$

where $\mathbf{S}_{noise} = \mathbf{G}\mathbf{S}_e\mathbf{G}^{\mathrm{T}}$, $\mathbf{S}_{cross-state} = \sum_{b\_ret} \mathbf{A}_{xs}\,\mathbf{S}_a^{b\_ret}\mathbf{A}_{xs}{}^{\mathrm{T}}$ and

$$\mathbf{S}_{systematic} = \sum_b \mathbf{G}\mathbf{K}_b\mathbf{S}_b(\mathbf{G}\mathbf{K}_b)^{\mathrm{T}} \quad (4)$$

In this notation, *b* variables are parameters that are held constant in the CO retrieval (such as temperature and water vapor), but affect the radiance observation and are propagated through Jacobian $\mathbf{K}_b$ while *b_ret* variables are retrieved along with CO (such as surface emissivity) and have corresponding off-diagonal terms in the full retrieval averaging kernel matrix. When we apply the satellite instrument operator in Eq. 1 to the in situ aircraft profile, we are accounting for the smoothing error term. Thus, we expect differences between $\hat{x}_{val}$ and our retrieved $\hat{x}$ to be due to observational error terms (Eq. 3) and to geophysical differences from the sampling of different airmasses and surface locations because of imperfect coincidence.

5. Validation Results

5.1 TROPESS/CrIS CO comparisons with NOAA GML aircraft data

After extending the in situ profiles vertically (described in Sec. 4.1) and applying Eq. 1, we compute the differences between satellite retrievals and transformed aircraft profiles. Figure 4 shows the bias (% relative difference) of the CrIS CO retrieved profiles with respect to NOAA GML aircraft profiles ($\hat{x}_{val}$). A similar pattern of positive bias in the lower to mid troposphere and negative bias in the upper troposphere is observed for MUSES/AIRS profiles compared to NOAA GML flights (Hegarty et al., 2022). However, MOPITT (version 9, TIR-only data) comparisons to NOAA GML (Deeter et al., 2022) have almost the opposite vertical bias pattern with a negative bias (-1.6 %) in the lower to middle troposphere and a positive bias (0.6 %) in the upper troposphere. Since TROPESS and MOPITT retrievals both use optimal estimation algorithms and a similar prior CO error covariance, this different vertical bias pattern is most likely due to instrument differences. MOPITT uses gas filter correlation radiometry instead of spectroscopy to detect CO absorption in the atmosphere with corresponding differences in vertical sensitivity that are determined from gas cell pressure rather than spectral resolution. After accounting for retrieval differences in a priori profiles and covariances between MOPITT and IASI (another FTS instrument), George et al. (2015) find a similar positive bias for MOPITT in the upper troposphere.

Table 2 gives the mean bias and standard deviations for selected pressures and partial column average VMR over different observing conditions (land, ocean, day and night). The partial column refers to the CO column between the minimum and maximum flight altitudes of each aircraft profile. The average VMR over this range is computed by interpolating both the CrIS retrieval and the aircraft $\hat{x}_{val}$ profile to these endpoints. Since aircraft flights normally occur during daytime, there are fewer coincident pairs for CrIS night retrievals. Tang et al. (2020) find larger bias and variance for nighttime MOPITT data in comparisons with in situ aircraft data, especially for flights over urban regions, suggesting more night validation flights are needed to properly evaluate night satellite retrievals.

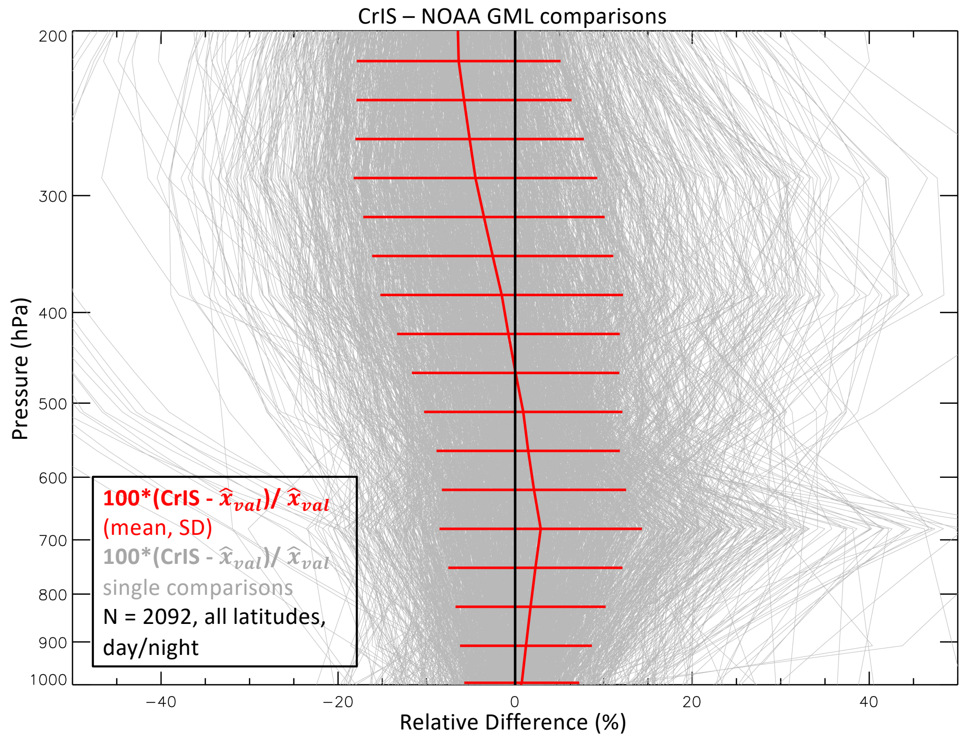

Figure 4. *Relative differences (%) in single CrIS retrievals with coincident NOAA GML $\hat{x}_{val}$ profiles (grey) and the average % difference with 1σ horizontal bars (red). Both day and night CrIS observations are included for coincidence search with 1866 day and 266 night comparison pairs found.*

Table 2. Bias and standard deviation (SD) for comparisons of SNPP TROPESS/CrIS CO retrievals and in situ CO profiles from NOAA GML fights.

Obs. type	% bias 750 hPa	% SD 750 hPa	% bias 511 hPa	% SD 511 hPa	% bias 287 hPa	% SD 287 hPa	% bias Column	% SD Column	# pairs
All	2.29	9.84	0.92	11.20	-4.48	13.76	0.57	8.56	2092
Land	3.04	10.85	-0.044	11.95	-6.15	13.97	1.24	9.46	853
Ocn	1.78	9.04	1.58	10.59	-3.33	13.49	0.11	7.84	1239
Day	1.97	9.79	0.13	10.93	-5.37	13.32	0.23	8.77	1866
Ngt	4.94	9.86	7.36	11.27	2.81	15.05	3.41	5.82	266

Figure 5 shows how the observed partial column average VMR and CrIS retrieval bias with respect to NOAA GML $\hat{x}_{val}$ profiles vary with latitude and Figure 6 shows how these vary with time. No significant bias dependence on latitude is observed for the NOAA GML flight sites. Although a bias drift of -0.007 ± 0.001 %/day is detected, we recognize that our comparison time range is not sufficient for a reliable estimate of bias drift, and more years of comparisons would be required.

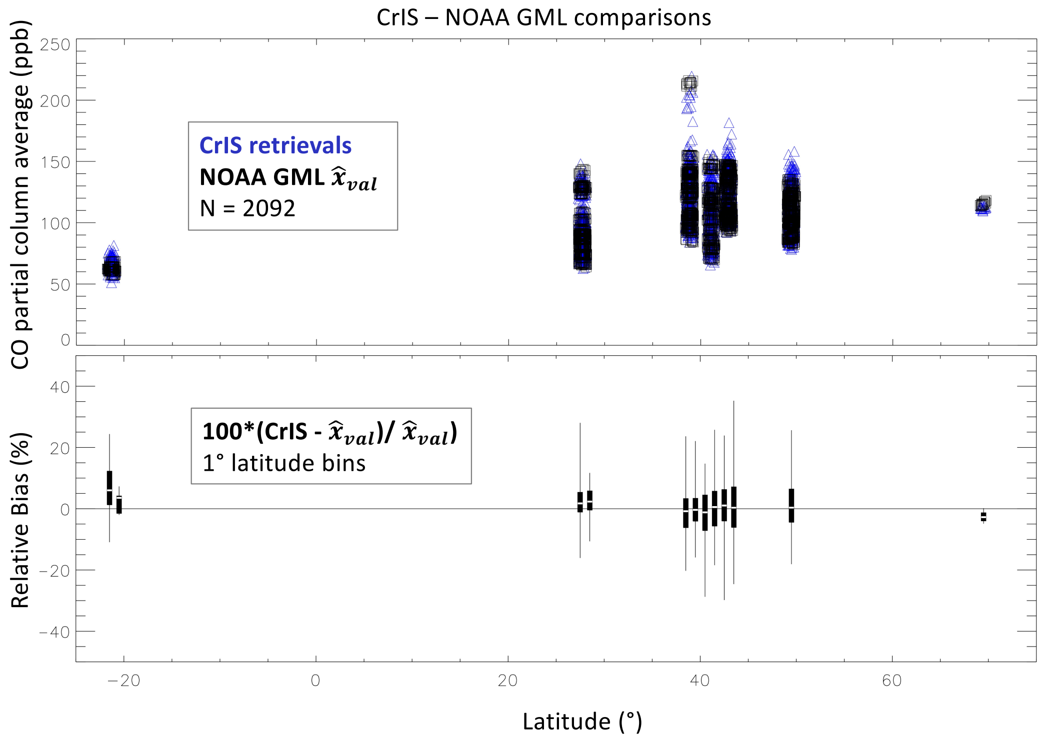

Figure 5. *Latitude dependence of CO partial column average VMR (ppb) for TROPESS/CrIS retrievals and NOAA GML* $\hat{x}_{val}$ *(upper panel) and bias difference statistics (lower panel) shown by box/whisker symbols representing minimum and maximum values (whisker), lower quartile (box bottom), median (white stripe), and upper quartile (box top). A minimum of 5 comparisons per bin was required.*

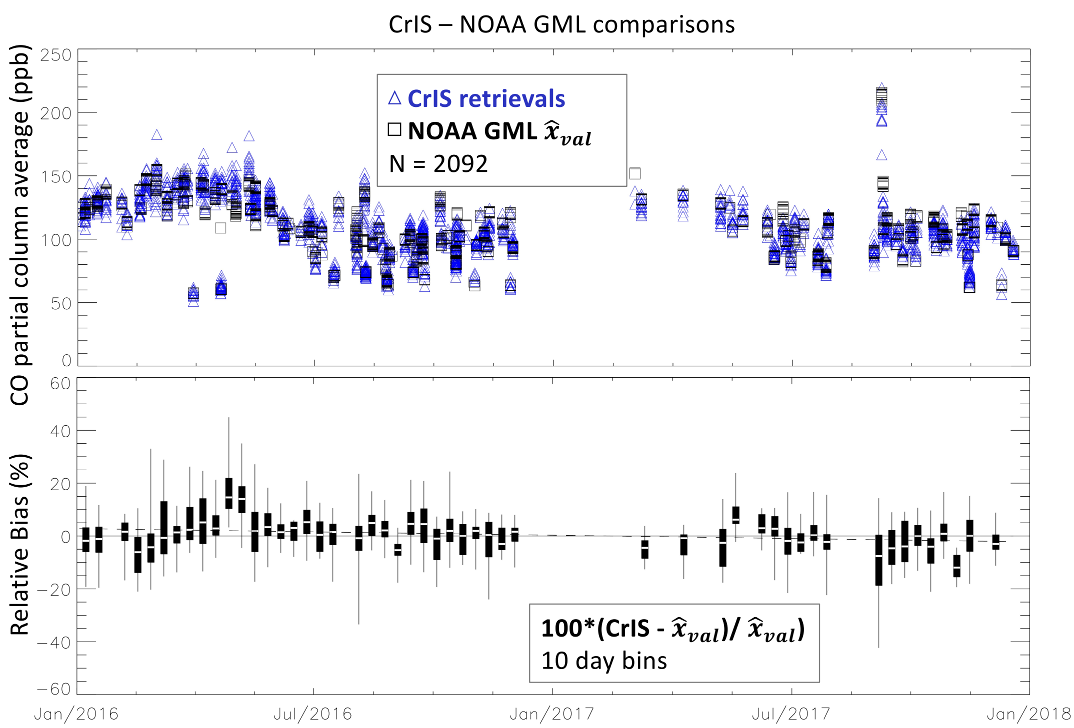

Figure 6. *Time dependence of CO partial column average VMR (ppb) for TROPESS/CrIS retrievals and NOAA GML* $\hat{x}_{val}$ *(upper panel) and bias difference statistics (lower panel) shown by box/whisker symbols representing minimum and maximum values (whisker), lower quartile (box bottom), median (white stripe), and upper quartile (box top). A minimum of 5 comparisons per bin was required. The dashed line indicates a fit for bias drift (see text).*

5.2 TROPESS/CrIS CO validation with ATom

Figure 7 shows the bias (% relative difference) of the CrIS CO retrieved profiles with respect to ATom $\hat{x}_{val}$ in situ profiles for all latitudes and 3 latitude ranges: 30°S to 30°N, 90°S to 30°S, and 30°N to 90°N. The vertical behavior of the bias is similar to the above CrIS comparisons with NOAA GML flights, with positive bias in the lower troposphere and negative bias in the upper troposphere and is also similar to the MUSES/AIRS CO profiles compared to ATom flights (Hegarty et al., 2022). However, for MOPITT V9T comparisons to ATom flights (Deeter et al., 2022), the vertical bias pattern is again mostly opposite, with a negative bias (~4 %) in the lower to mid troposphere and a positive bias (~2 %) in the upper troposphere. This TROPESS/CrIS CO bias also differs from Nalli et al. (2020) who examined the bias of NUCAPS profiles (including CO) with respect to ATom in situ profiles. That study, using the multiple FOV NUCAPS retrievals, found a small positive bias (~2%) for SNPP/CrIS CO with respect to ATom CO at all tropospheric vertical levels after applying their averaging kernels.

CrIS CO comparisons with ATom have less variance than comparisons with NOAA GML, especially for 90°S to 30°S. Table 3 gives the mean bias and standard deviations for selected pressures and partial column average VMR over different observing conditions (land, ocean, day and night) and latitude ranges. As described above, the partial column average VMR is computed over the altitude ranges of each aircraft profile. Due to the nature of the ATom campaign, there are fewer observations over land.

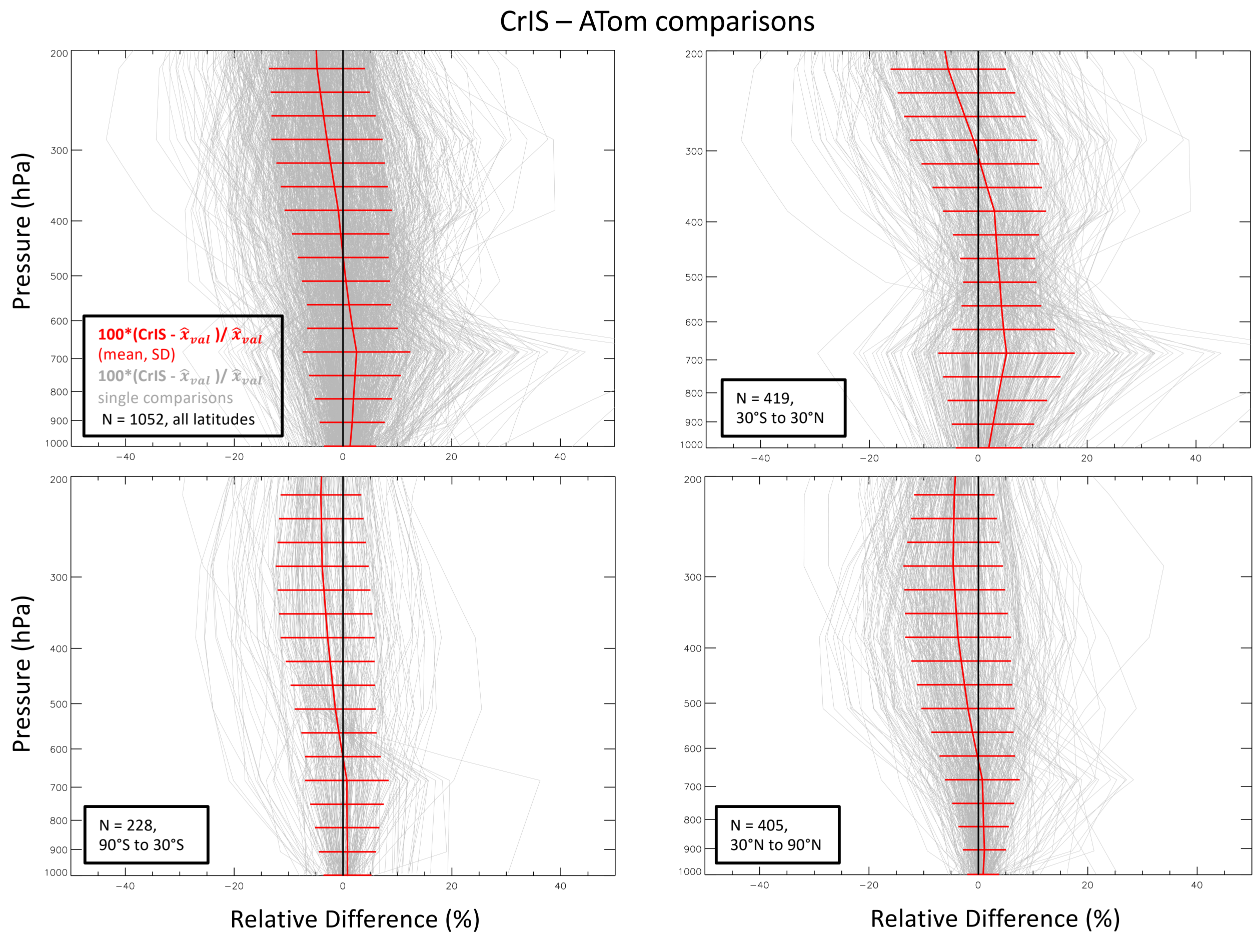

***Figure** 7. Relative differences (%) in single CrIS retrievals with coincident ATom $\hat{x}_{val}$ profiles (grey) and the average % difference with 1σ horizontal bars (red). Latitude ranges are indicated in each panel along with the number of comparison pairs. Both day and night CrIS observations are included.*

Figure 8 shows how the observed partial column average VMRs and CrIS retrieval bias with respect to ATom $\hat{x}_{val}$ profiles vary with latitude. It appears that tropical and northern hemisphere sub-tropical latitude ranges have a slightly higher positive bias than what is observed for higher latitudes, potentially indicating a TROPESS/CrIS retrieval issue with water vapor or some other interferent that is not fully characterized and requires further investigation. For example, Deeter et al. (2018) found that an empirical correction to MOPITT radiances resulting from a linear dependence on water vapor removed most of the latitude dependent bias in MOPITT CO profiles. Another gas interferent in the TIR CO band is N_2O and we will also need to consider the latitude dependent N_2O anomalies observed by ATom (Gonzalez et al., 2021) when assessing the contributions to this latitude dependence in TROPESS/CrIS CO bias.

Table 3. Bias and standard deviation (SD) for comparisons of SNPP TROPESS/CrIS CO retrievals and in situ CO profiles from ATom flight campaigns 1-4.

Obs. type	Latitude Range (°)	% bias 750 hPa	% SD 750 hPa	% bias 511 hPa	% SD 511 hPa	% bias 287 hPa	% SD 287 hPa	% bias Col.	% SD Col.	# pairs
All	all	2.21	8.46	0.54	8.12	-2.95	10.24	-0.035	5.91	1052
Land	all	1.20	4.15	-0.49	7.59	-2.95	10.46	-0.79	7.09	102
Land	30S-30N	-	-	-	-	-	-	-	-	1
Land	30N-90N	1.22	4.27	-0.69	7.76	-3.25	10.70	-0.91	7.32	95
Land	90S-30S	0.12	0.29	0.89	2.35	1.84	4.65	0.67	1.86	6
Ocn	all	2.32	8.79	0.65	8.17	-2.95	10.21	0.046	5.76	950
Ocn	30S-30N	4.32	10.80	3.96	6.75	-0.86	11.67	2.33	5.44	418
Ocn	30N-90N	0.75	6.01	-2.28	8.70	-5.03	8.51	-2.22	6.34	310
Ocn	90S-30S	0.74	6.85	-1.46	7.5	-3.98	8.57	-1.09	3.49	222
Day	all	2.62	8.76	0.53	7.91	-3.21	9.81	0.010	5.85	782
Day	30S-30N	4.94	11.42	3.55	6.57	-2.01	10.99	2.23	5.16	300
Day	30N-90N	0.91	5.76	-1.63	8.62	-4.33	9.22	-1.68	6.74	331
Day	90S-30S	1.79	6.90	-0.72	6.71	-3.11	8.12	-0.70	2.91	151
Ngt	all	1.03	7.39	0.57	8.71	-2.21	11.36	-0.17	6.08	270
Ngt	30S-30N	2.79	8.82	5.02	7.07	2.03	12.73	2.59	6.09	119
Ngt	30N-90N	0.68	5.15	-3.16	7.93	-5.88	8.45	-2.98	5.84	74
Ngt	90S-30S	-1.35	5.94	-2.73	8.58	-5.25	9.15	-1.73	4.30	77

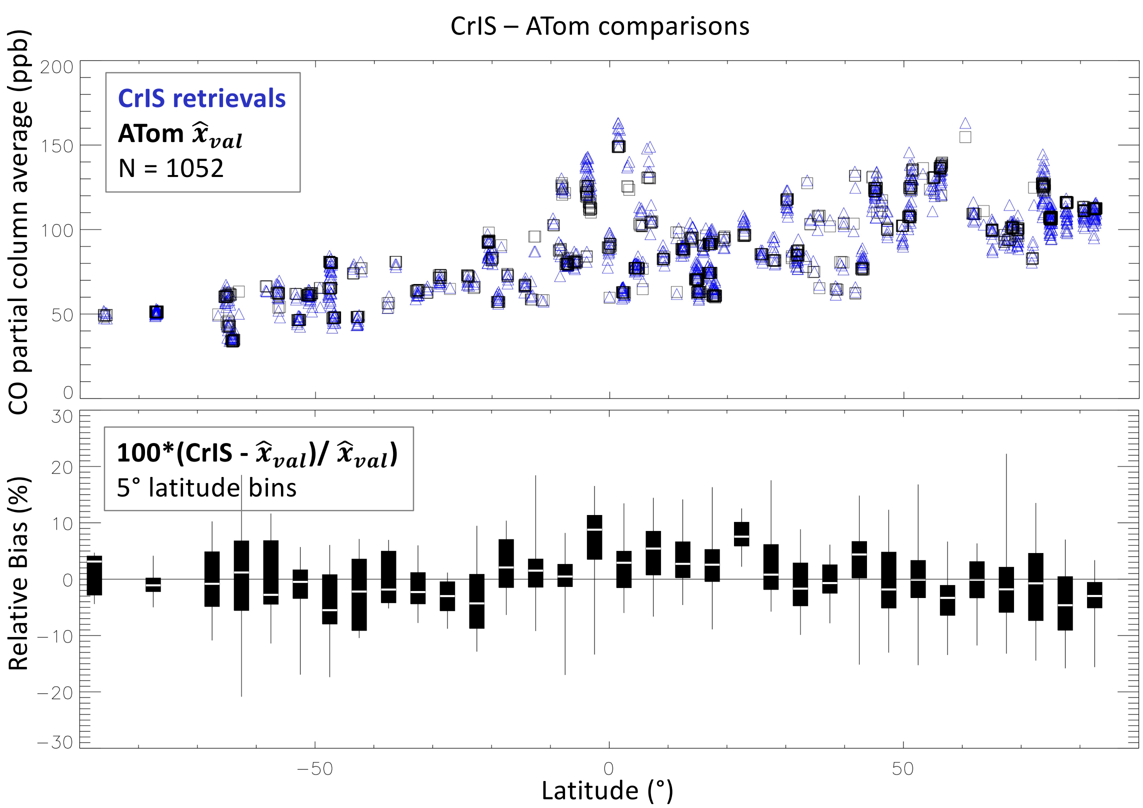

Figure 8. *Latitude dependence of CO partial column average VMR (ppb) for TROPESS/CrIS retrievals and ATom $\hat{x}_{val}$ (upper panel) and bias difference statistics (lower panel) shown by box/whisker symbols representing minimum and maximum values (whisker), lower quartile (box*

bottom), median (white stripe), and upper quartile (box top). A minimum of 5 comparisons per bin was required.

In Figure 9, we examine the seasonal behavior of CO sampled by ATom and CrIS in mostly remote ocean regions. In the high latitude southern hemisphere (SH), we see the lowest values in summer and fall (Jan/Feb and Apr/May) as expected due to the chemical destruction of CO in a region with few local combustion sources. In the tropics, we find high values corresponding to African and South American biomass burning plumes over the Atlantic in all seasons except Northern Hemisphere (NH) spring. Lower values of CO in the tropics for NH summer and winter correspond to profiles over the Pacific ocean (e.g., Strode et al., 2018, Bourgeois et al., 2020). The close alignment of the CrIS and ATom $\hat{x}_{val}$ partial column average values in Fig. 9 indicates that CrIS is able to capture the seasonal, latitudinal and hemispherical variations observed by ATom.

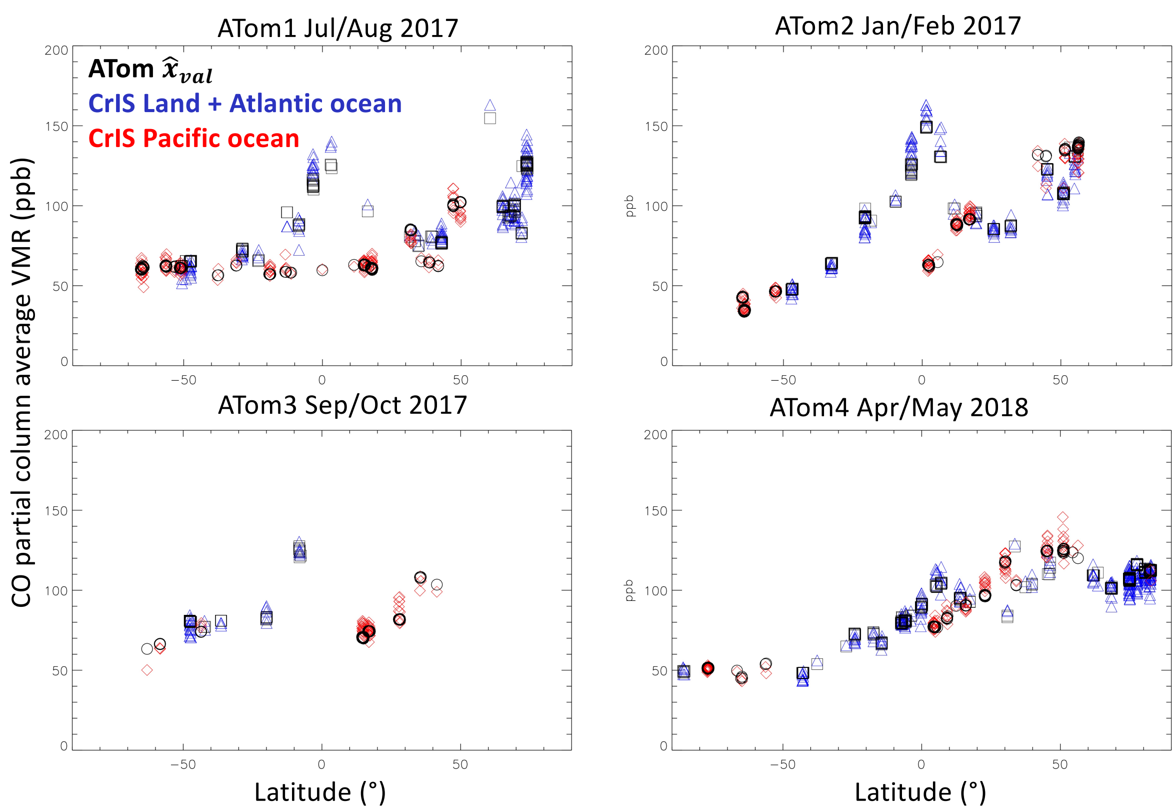

***Figure 9**. Latitude dependence of partial column average CO for each ATom campaign. Black squares ATom $\hat{x}_{val}$ partial column average values over Atlantic Ocean scenes; black circles indicate ATom values over Pacific Ocean scenes. Blue triangles indicate CrIS CO partial column average values over land and Atlantic Ocean scenes; red diamonds indicate CrIS values over Pacific Ocean scenes.*

5.3 Dependence on CO amount

For both the NOAA GML and ATom flights we find a small negative dependence of TROPESS/CrIS retrieval bias with respect to CO amount, with magnitude less than 0.1 %/ppb. Figure 10 shows how the partial column average VMR bias varies with CO VMR for the two validation data sources and we can also see how ATom flights sampled air with lower CO concentrations. Figure 10 indicates that TROPESS/CrIS CO average column VMRs have very little dependence on CO amount and we find similar results for CrIS retrieved CO at vertical levels 511 hPa and 750 hPa (shown in the supplementary material).

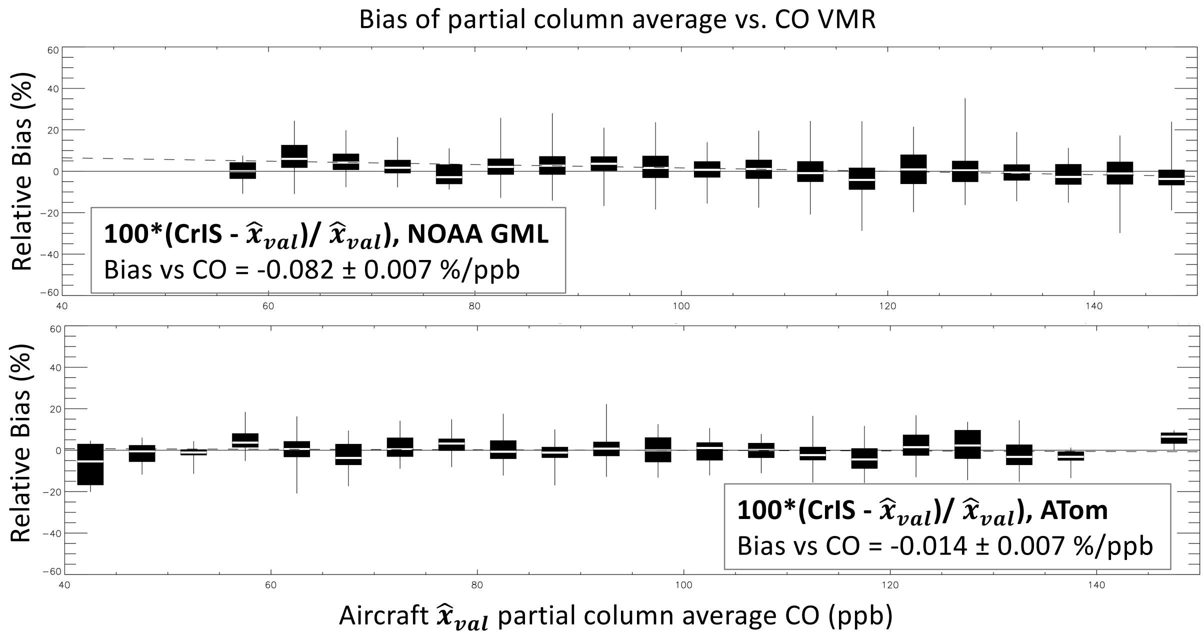

Figure 10. *Bias of CrIS partial column average CO vs CO amount for NOAA GML flights in top panel and ATom flights in bottom panel with box/whisker symbols in 5 ppb bins. Linear regression results are shown in the legend boxes.*

5.4 Evaluation of TROPESS/CrIS CO retrieval observational errors

Here we compare the observed variance of differences between retrieved CrIS CO profiles and in situ aircraft profiles, after applying Eq. 1, with the TROPESS reported observational errors defined in Eqs. 3 and 4. As described in section 4.3, we expect the differences between retrieved CrIS and aircraft CO profiles ($\hat{x}_{val}$) to have a variance due to the combination of observational errors and geophysical variation from imperfect coincidence. Figure 11 shows comparisons of individual and average computed observational fractional errors to the standard deviation (SD) of CrIS – $\hat{x}_{val}$ profile differences as well as the diagonal for the a priori covariance and the SD of prior – $\hat{x}_{val}$ profile differences. As expected, the average observational errors are less than SD(CrIS – $\hat{x}_{val}$), but in some vertical ranges, they are much less and could be underestimated via instrument and systematic error assumptions in the TROPESS retrieval as Hegarty et al. (2022) suggest. Additional studies to test the sensitivity of the comparison variance to a range of coincidence criteria are needed to confirm a retrieval underestimate, but these would require several repeated validation measurements for the same observing conditions.

Despite the potential for underestimated observational errors, the general behavior of the error comparison is what we expect from Equation 1, and we can see the retrieval influence on the shape of SD(CrIS – $\hat{x}_{val}$). Near the surface, where there is less retrieval sensitivity as indicated by the averaging kernel, we see that SD(prior – $\hat{x}_{val}$) becomes smaller than SD(CrIS – $\hat{x}_{val}$).

This is expected for vertical ranges with less retrieval sensitivity since the priori contribution becomes more dominant in $\hat{x}_{val}$. In contrast, for the middle troposphere where we have the most sensitivity for TIR remote sensing, it is clear that SD(CrIS – $\hat{x}_{val}$) represents an improvement over SD(prior – $\hat{x}_{val}$). In Figure 12, the error comparison is shown separately for 3 ATom latitude ranges and we can see that the agreement between observational errors and SD(CrIS – $\hat{x}_{val}$) is closest for ATom flights in the mostly clean middle to high latitude southern hemisphere, where it is most likely that the aircraft and satellite are observing similar airmasses with background CO concentrations. These results give confidence that TROPESS single retrieval error characterization can be used to weight data for averaging and inverse analysis applications.

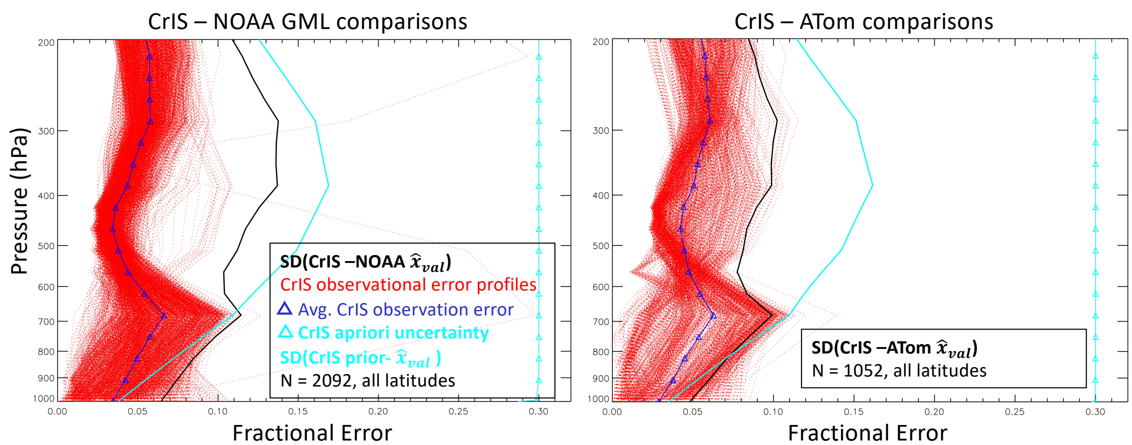

Figure 11. *Error comparison of CrIS observational error estimates and the standard deviation (SD) of CrIS- $\hat{x}_{val}$ (in black) for NOAA GML flights in the left panel and ATom flights in the right panel. Single profile CrIS observational error estimates are plotted in red, with average in dark blue with triangles. For reference, and the standard deviation of CrIS prior with aircraft $\hat{x}_{val}$ is in cyan and the apriori fractional uncertainty (0.3) is shown in cyan with triangles.*

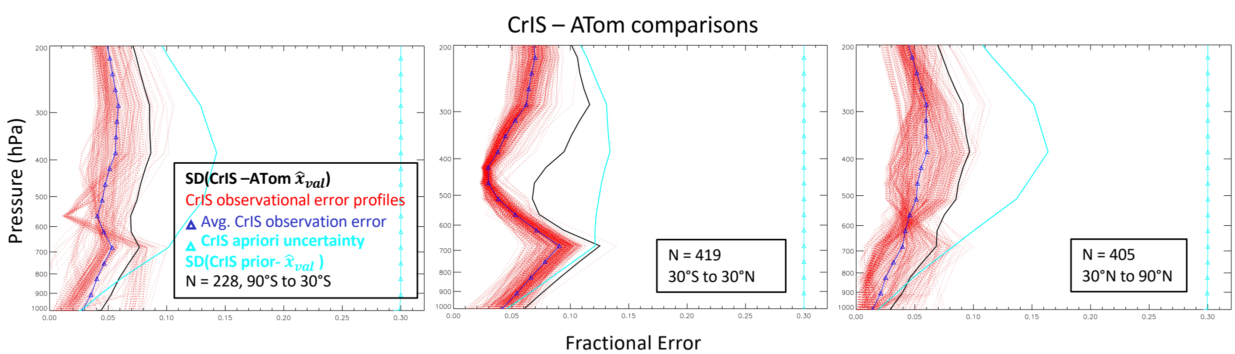

Figure 12. *Same as Fig. 11 but for 3 ATom latitude ranges.*

6. Summary and Conclusions

This study used in situ observations from routine NOAA GML flights and the four ATom campaigns to evaluate TROPESS single pixel CO retrievals from the SNPP/CrIS FTS instrument. We find that:

1) The single FOV CrIS product provides improved representation of CO in smoke plumes compared to retrievals that combine multiple FOVs.
2) Comparisons with aircraft in situ profiles (after extension, interpolation and application of Eq. 1) show that biases have a vertical dependence in the troposphere that is consistent for both sets of in situ data with average biases that are positive (~ 2.3 %) in the lower troposphere and negative (~ -4.5 %) in the upper troposphere.
3) Small biases (0.6 % and -0.04 % for NOAA GML and ATom, respectively) are observed for the CrIS CO partial column average VMR corresponding to the aircraft profile vertical ranges.
4) No significant latitude dependence of CrIS CO column bias is found for the NOAA GML comparisons, but comparisons with ATom, which better covered a range of latitudes, have a slightly more positive bias for tropical scenes that could indicate a small, uncharacterized retrieval dependence on water vapor or another interferent species.
5) CrIS CO retrievals capture the seasonal and spatial variations observed by ATom.
6) There is a small negative dependence (magnitude < 0.1 %/ppb) of CrIS bias on CO amount.
7) Comparisons of computed observational errors and standard deviations of retrieval-aircraft comparison differences show expected vertical behavior and demonstrate significant improvement over the standard deviation of prior-aircraft differences in vertical ranges with higher retrieval sensitivity.

TROPESS/CrIS CO biases detected in this study are in general much smaller than comparison standard deviations. We therefore make no recommendations for automated bias corrections in data processing, similar to other validation studies for satellite CO retrievals (e.g., Deeter et al, 2019; 2022). This is unlike other TROPESS products such as CH_4 (Kulawik et al., 2021) where a bias correction is more appropriate given the size of bias detected as well as the atmospheric lifetime (~10 years for methane) and reduced atmospheric variability compared to CO. Each analysis using TROPESS/CrIS CO data must consider the variability of CO over the domain of interest and ascertain whether the biases observed here could affect numerical conclusions. The biases reported from this study will need to be included when long term records of satellite CO observations are harmonized and used together for computing trends, data assimilation or other analyses. For example, with the 22-year record of MOPITT CO profiles, this is especially important when combining datasets since the vertical bias pattern for MOPITT data with respect to in situ observations has a positive bias in the upper troposphere and negative bias in the lower to middle troposphere with the opposite behavior compared to the TROPESS/CrIS vertical bias pattern.

Future validation of the TROPESS/CrIS CO products will include a longer time record of comparisons and quantification of bias drift, for CrIS on SNPP and on the JPSS satellite series. The validation results presented here demonstrate that these products are suitable for tropospheric CO data analyses. The bias at all vertical levels is <10 % and error characterization for single retrievals can be used to weight data for averaging and applications such as data assimilation and inverse modelling.

Data availability. The NOAA GML data were obtained from https://doi.org/10.7289/V5N58JMF (Sweeney et al. 2021). The ATom aircraft data were obtained from https://doi.org/10.3334/ORNLDAAC/1581 (Wofsy et al., 2018). TROPESS/CrIS CO products are available via the GES DISC from the NASA TRopospheric Ozone and its Precursors from Earth System Sounding (TROPESS) project at https://doi.org/10.5067/I1NONOEPXLHS (Bowman, 2021). The CrIS–aircraft matched data set used here for validation is available from the authors on request.

Author contributions. HMW, GLF, SSK, JDH, KCP, ML and VHP designed the study and HMW prepared the manuscript. GLF analyzed the satellite/aircraft comparisons and prepared the figures, SSK, KB, DF, VK, ML, KCP, VHP, JRW developed the MUSES algorithm and provided the CrIS CO retrievals. RC and KM participated in the ATom campaign and provided guidance in the use of the measurements. KM provided the NOAA GML aircraft data. All authors reviewed and edited the manuscript.

Competing Interests. Some authors are members of the editorial board of AMT. The peer-review process was guided by an independent editor, and the authors have no other competing interests to declare.

Acknowledgements. This research was conducted at the National Center for Atmospheric Research (NCAR), which is sponsored by the National Science Foundation. Part of this research was carried out at the Jet Propulsion Laboratory (JPL), California Institute of Technology, under a contract with the National Aeronautics and Space Administration. The NOAA GML aircraft observations are supported by NOAA and CIRES. The ATom aircraft data were supported by the NASA Airborne Science Program and Earth Science Project Office. We acknowledge the use of imagery from the NASA Worldview application (*https://worldview.earthdata.nasa.gov/*), part of the NASA Earth Observing System Data and Information System (EOSDIS). We thank Dr. Benjamin Gaubert for his NCAR internal review of the manuscript.

Financial support. The Jet Propulsion Laboratory (JPL), California Institute of Technology, is under a contract with the National Aeronautics and Space Administration (80NM0018D0004). This research has also been supported by NASA via the TRopospheric Ozone and its Precursors from Earth System Sounding (TROPESS) project at JPL and a NASA ROSES award: 80NSSC18K0687. The NOAA Cooperative Agreement with CIRES is NA17OAR4320101. The NCAR facility is sponsored by the National Science Foundation (grant no. 1852977).

References

Barnet, C (2019), Sounder SIPS: Suomi NPP CrIMSS Level 2 CLIMCAPS Full Spectral Resolution: Atmosphere cloud and surface geophysical state V2, Greenbelt, MD, USA, Goddard Earth Sciences Data and Information Services Center (GES DISC), Last Accessed: **[*2022.03.23*]**, 10.5067/62SPJFQW5Q9B

Beer, R.: TES on the Aura mission: Scientific objectives, measurements, and analysis overview, *IEEE Transactions on Geoscience and Remote Sensing*, vol. 44, no. 5, pp. 1102-1105, doi:10.1109/TGRS.2005.863716, 2006.

Borsdorff, T., J. Aan de Brugh, H. Hu, I. Aben, O. Hasekamp, and J. Landgraf, Measuring Carbon Monoxide With TROPOMI: First Results and a Comparison With ECMWF-IFS Analysis Data, *Geophysical Research Letters*, *45*(6), 28262832, doi:10.1002/2018GL077045, 2018.

Bourgeois, I., Peischl, J., Thompson, C. R., Aikin, K. C., Campos, T., Clark, H., Commane, R., Daube, B., Diskin, G. W., Elkins, J. W., Gao, R.-S., Gaudel, A., Hintsa, E. J., Johnson, B. J., Kivi, R., McKain, K., Moore, F. L., Parrish, D. D., Querel, R., Ray, E., Sánchez, R., Sweeney, C., Tarasick, D. W., Thompson, A. M., Thouret, V., Witte, J. C., Wofsy, S. C., and Ryerson, T. B.: Global-scale distribution of ozone in the remote troposphere from the ATom and HIPPO airborne field missions, Atmos. Chem. Phys., 20, 10611–10635, https://doi.org/10.5194/acp-20-10611-2020, 2020.

Bowman, K. W., Rodgers, C. D., Kulawik, S. S., Worden, J., Sarkissian, E., Osterman, G., Steck, T., Lou, M., Eldering, A. and Shephard, M.: Tropospheric emission spectrometer: retrieval method and error analysis, *IEEE Transactions on Geoscience and Remote Sensing*, vol. 44, no. 5, pp. 1297-1307, doi:10.1109/TGRS.2006.871234, 2006.

Bowman, K. W. et al., TROPESS Level 2 Algorithm Theoretical Basis Document (ATBD) V1, 2021 at: https://docserver.gesdisc.eosdis.nasa.gov/public/project/TROPESS/TROPESS_ATBDv1.1.pdf Last accessed: 2022.04.12

Bowman, K. W., TROPESS CrIS-SNPP L2 Carbon Monoxide for West Coast Fires HiRes, Standard Product V1, Greenbelt, MD, USA, Goddard Earth Sciences Data and Information Services Center (GES DISC), Accessed: 2022.02.02**,** 10.5067/Y3MAIEUNDTBX, 2021

Brasseur, G. P., Hauglustaine, D. A., Walters, S., Rasch, P. J., Muller, J. F., Granier, C., and Tie, X. X.: MOZART, a global chemical transport model for ozone and related chemical trac- ers 1. Model description, J. Geophys. Res., 103, 28265–28289, 1998.

Buchholz, R. R., Worden, H. M., Park, M., Francis, G. Deeter, M. N., Edwards, D. P., Emmons, L. K., Gaubert, B., Gille, J., Martinez-Alonso, S., Tang, W., Kumar, R., Drummond, J. R., Clerbaux, C., George, M., Coheur, P-F., Hurtmans, D., Bowman, K. W., Luo, M., Payne, V. H., Worden, J. R., Chin, M., Levy, R. C., Warner, J., Wei, Z., Kulawik, S. S.: Air pollution trends measured from Terra: CO and AOD over industrial, fire-prone and background regions, Remote Sensing of the Environment., 256, doi.org/10.1016/j.rse.2020.112275, 2021.

Byrne, B., Liu, J., Lee, M., Yin, Y., Bowman, K. W., Miyazaki, K., et al.: The Carbon Cycle of Southeast Australia During 2019–2020: Drought, Fires, and Subsequent Recovery. AGU Advances, 2(4). https://doi.org/10.1029/2021av000469, 2021.

Clerbaux, C., Boynard, A., Clarisse, L., George, M., Hadji-Lazaro, J., Herbin, H., Hurtmans, D., Pommier, M., Razavi, A., Turquety, S., Wespes, C., and Coheur, P.-F.: Monitoring of atmospheric composition using the thermal infrared IASI/MetOp sounder, Atmos. Chem. Phys., 9, 6041–6054, doi:10.5194/acp-9-6041-2009, 2009.

Deeter, M. N., D. P. Edwards, J. C. Gille, L. K. Emmons, G. Francis, S.-P. Ho, D. Mao, D. Masters, H. Worden, J. R. Drummond, and P. C. Novelli, The MOPITT version 4 CO product: Algorithm enhancements, validation, and long-term stability, *J. Geophys. Res.-Atmos.*, *115*(D7), doi:10.1029/2009JD013005, 2010.

Deeter, M. N., D. P. Edwards, G. L. Francis, J. C. Gille, D. Mao, S. Martinez-Alonso, H. M. Worden, D. Ziskin, and M. O. Andreae, Radiance-based retrieval bias mitigation for the MOPITT instrument: the version 8 product, *Atmos. Meas. Tech.*, *12*(8), 4561–4580, doi:10.5194/amt-12-4561-2019, 2019.

Deeter, M., Francis, G., Gille, J., Mao, D., Martínez-Alonso, S., Worden, H., Ziskin, D., Drummond, J., Commane, R., Diskin, G., and McKain, K.: The MOPITT Version 9 CO product: sampling enhancements and validation, Atmos. Meas. Tech., 15, 2325–2344, https://doi.org/10.5194/amt-15-2325-2022, 2022.

de Laat, A. T. J., Gloudemans, A. M. S., Schrijver, H., van den Broek, M. M. P., Meirink, J. F., Aben, I., and Krol, M.: Quantitative analysis of SCIAMACHY carbon monoxide total column measurements, Geophys. Res. Lett., 33, L07807, doi:10.1029/2005GL025530, 2006.

Drummond, J. R., J. Zou, F. Nichitiu, J. Kar, R. Deschambaut, and J. Hackett, A review of 9-year performance and operation of the MOPITT instrument, *J. Adv. Space Res.*, doi:10.1016/j.asr.2009.11.019, 2010.

Edwards, D. P., Emmons, L. K., Hauglustaine, D. A., Chu, A., Gille, J. C., Kaufman, Y. J., P´etron, G., Yurganov, L. N., Giglio, L., Deeter, M. N., Yudin, V., Ziskin, D. C.,Warner, J., Lamarque, J.-F., Francis, G. L., Ho, S. P., Mao, D., Chan, J., and Drummond, J. R.: Observations of Carbon Monoxide and Aerosol From the Terra Satellite: Northern Hemisphere Variability, J. Geophys. Res., 109, D24202, doi:10.1029/2004JD0047272004, 2004.

Edwards, D. P., Emmons, L. K., Gille, J. C., Chu, A., Atti´e, J.-L., Giglio, L., Wood, S. W., Haywood, J., Deeter, M. N., Massie, S. T., Ziskin, D. C., and Drummond, J. R.: Satellite observed pollution from Southern Hemisphere biomass burning, J. Geophys. Res., 111, 14312, doi:10.1029/2005JD006655, 2006.

Eldering, A., S. S. Kulawik, J. Worden, K. Bowman, and G. Osterman, Implementation of cloud retrievals for TES atmospheric retrievals: 2. Characterization of cloud top pressure and effective optical depth retrievals, J. Geophys. Res., 113, D16S37, doi:10.1029/2007JD008858, 2008.

Fu, D., Bowman, K. W., Worden, H. M., Natraj, V., Worden, J. R., Yu, S., Veefkind, P., Aben, I., Landgraf, J., Strow, L., and Han, Y.: High-resolution tropospheric carbon monoxide profiles retrieved from CrIS and TROPOMI, Atmos. Meas. Tech., 9, 2567-4572579, https://doi.org/10.5194/amt-9-2567-2016, 2016.

Fu, D., Kulawik, S. S., Miyazaki, K., Bowman, K. W., Worden, J. R., Eldering, A., Livesey, N. J., Teixeira, J., Irion, F. W., Herman, R. L., Osterman, G. B., Liu, X., Levelt, P. F., Thompson, A. M., and Luo, M.: Retrievals of tropospheric ozone profiles from the synergism of AIRS and OMI: methodology and validation, Atmospheric Measurement Techniques, 11(10), 5587–5605, doi:10.5194/amt-11-5587-2018-supplement, 2018.

Fu D., Millet D.B., Wells K.C., Payne V.H., Yu S., Guenther A., and Eldering A.: Direct retrieval of isoprene from satellite based infrared measurements, Nature Communication, 10.3811, doi:10.1038/s41467-019-11835-0. 2019.

Gambacorta, A., C. Barnet, W. Wolf, T. King, E. Maddy, L. Strow, X. Xiong, N. Nalli, and M. Goldberg An Experiment Using High Spectral Resolution CrIS Measurements for Atmospheric Trace Gases:

Carbon Monoxide Retrieval Impact Study, *IEEE Geoscience and Remote Sensing Letters*, *11*(9), 16391643, doi:10.1109/LGRS.2014.2303641, 2014.

Gambacorta, A., Nalli, N.R., Barnet, C.D., Tan, C., Iturbide-Sanchez, F., and Zhang, K: *The NOAA Unique Combined Atmospheric Processing System (NUCAPS): Algorithm Theoretical Basis Document (ATBD)*; ATBD v2.0; NOAA/NESDIS/STAR Joint Polar Satellite System: College Park, MD, USA, 2017.

Gaubert, B., A. F. Arellano, J. Barré, H. M. Worden, L. K. Emmons, S. Tilmes, R. R. Buchholz, F. Vitt, K. Raeder, N. Collins, J. L. Anderson, C. Wiedinmyer, S. Martinez Alonso, D. P. Edwards, M. O. Andreae, J. W. Hannigan, C. Petri, K. Strong, and N. Jones, Toward a chemical reanalysis in a coupled chemistry-climate model: An evaluation of MOPITT CO assimilation and its impact on tropospheric composition, *J. Geophys. Res. Atmos.*, *121*(12), 2016JD024863, doi:10.1002/2016JD024863, 2016.

Gaubert, B., H. M. Worden, A. F. J. Arellano, L. K. Emmons, S. Tilmes, J. Barre, S. M. Alonso, F. Vitt, J. L. Anderson, F. Alkemade, S. Houweling, and D. P. Edwards, Chemical Feedback From Decreasing Carbon Monoxide Emissions, *Geophys. Res. Lett.*, *44*(19), 99859995, doi:10.1002/2017GL074987, 2017.

Gaubert, B., Emmons, L. K., Raeder, K., Tilmes, S., Miyazaki, K., Arellano Jr., A. F., Elguindi, N., Granier, C., Tang, W., Barré, J., Worden, H. M., Buchholz, R. R., Edwards, D. P., Franke, P., Anderson, J. L., Saunois, M., Schroeder, J., Woo, J.-H., Simpson, I. J., Blake, D. R., Meinardi, S., Wennberg, P. O., Crounse, J., Teng, A., Kim, M., Dickerson, R. R., He, H., Ren, X., Pusede, S. E., and Diskin, G. S.: Correcting model biases of CO in East Asia: impact on oxidant distributions during KORUS-AQ, Atmos. Chem. Phys., 20, 14617–14647, https://doi.org/10.5194/acp-20-14617-2020, 2020.

George, M., Clerbaux, C., Bouarar, I., Coheur, P.-F., Deeter, M. N., Edwards, D. P., Francis, G., Gille, J. C., Hadji-Lazaro, J., Hurtmans, D., Inness, A., Mao, D., and Worden, H. M.: An examination of the long-term CO records from MOPITT and IASI: comparison of retrieval methodology, Atmos. Meas. Tech., 8, 4313–4328, https://doi.org/10.5194/amt-8-4313-2015, 2015.

Gonzalez, Y., Commane, R., Manninen, E., Daube, B. C., Schiferl, L. D., McManus, J. B., McKain, K., Hintsa, E. J., Elkins, J. W., Montzka, S. A., Sweeney, C., Moore, F., Jimenez, J. L., Campuzano Jost, P., Ryerson, T. B., Bourgeois, I., Peischl, J., Thompson, C. R., Ray, E., Wennberg, P. O., Crounse, J., Kim, M., Allen, H. M., Newman, P. A., Stephens, B. B., Apel, E. C., Hornbrook, R. S., Nault, B. A., Morgan, E., and Wofsy, S. C.: Impact of stratospheric air and surface emissions on tropospheric nitrous oxide during ATom, Atmos. Chem. Phys., 21, 11113–11132, https://doi.org/10.5194/acp-21-11113-2021, 2021.

Hegarty, J., Mao, H., and Talbot, R.: Synoptic influences on springtime tropospheric O_3 and CO over the North American export region observed by TES, Atmos. Chem. Phys., 9, 3755–3776, doi.org/10.5194/acp-9-3755-2009, 2009.

Hegarty, J., Mao, H., and Talbot, R.: Winter- and summertime continental influences on tropospheric O_3 and CO observed by TES over the western North Atlantic Ocean, Atmos. Chem. Phys., 10, 3723–3741, doi.org/10.5194/acp-10-3723-2010, 2010.

Hegarty, J. D., Cady-Pereira, K. E., Payne, V. H., Kulawik, S. S., Worden, J. R., Kantchev, V., Worden, H. M., McKain, K., Pittman, J. V., Commane, R., Daube Jr., B. C., and Kort, E. A.: Validation and error estimation of AIRS MUSES CO profiles with HIPPO, ATom, and NOAA GML aircraft observations, Atmos. Meas. Tech., 15, 205–223, https://doi.org/10.5194/amt-15-205-2022, 2022.

Holloway, T., Levy II, H., Kasibhatla, P., Global distribution of carbon monoxide, J. Geophys. Res. 105 (D10), 12,123–12,147. https://doi.org/10.1029/1999JD901173, 2000.

Inness, A., M. Ades, A. Agustí-Panareda, J. Barré, A. Benedictow, A.-M. Blechschmidt, J. J. Dominguez, R. Engelen, H. Eskes, J. Flemming, V. Huijnen, L. Jones, Z. Kipling, S. Massart, M. Parrington, V.-H. Peuch, M. Razinger, S. Remy, M. Schulz, and M. Suttie, The CAMS reanalysis of atmospheric composition, *Atmospheric Chemistry and Physics*, *19*(6), 35153556, doi:https://doi.org/10.5194/acp-19-3515-2019, 2019.

Jiang, Z., Worden, J. R., Worden, H., Deeter, M., Jones, D. B. A., Arellano, A. F., and Henze, D. K.: A 15-year record of CO emissions constrained by MOPITT CO observations, Atmos. Chem. Phys., 17, 4565–4583, doi.org/10.5194/acp-17-4565-2017, 2017.

Jones, Dylan B. A., Kevin W. Bowman, Paul I. Palmer, John R. Worden, Daniel J. Jacob, Ross N. Hoffman, Isabelle Bey, and Robert M. Yantosca, Potential of Observations from the Tropospheric Emission Spectrometer to Constrain Continental Sources of Carbon Monoxide, *J. Geophys. Res. - Atmospheres, Vol.108, No. D24, 4789*, 10.1029/2003JD003702 , 2003.

Juncosa Calahorrano, J. F., Payne, V. H., Kulawik, S., Ford, B., Flocke, F., Campos, T., & Fischer, E. V. Evolution of acyl peroxynitrates (PANs) in wildfire smoke plumes detected by the Cross-Track Infrared Sounder (CrIS) over the western U.S. during summer 2018. *Geophysical Research Letters*, *48*, e2021GL093405. https://doi. org/10.1029/2021GL093405, 2021.

Karion, A., Sweeney, C., Tans, P., and Newberger, T.: AirCore: An Innovative Atmospheric Sampling System, Journal OF Atmospheric and Oceanic Technology, 27, 1839–1853, https://doi.org/10.1175/2010JTECHA1448.1, 2010.

Kopacz, M., Jacob, D. J., Fisher, J. A., Logan, J. A., Zhang, L.,Megretskaia, I. A., Yantosca, R. M., Singh, K., Henze, D. K.,Burrows, J. P., Buchwitz, M., Khlystova, I., McMillan, W. W.,Gille, J. C., Edwards, D. P., Eldering, A., Thouret, V., and Nedelec, P.: Global estimates of CO sources with high resolution by adjoint inversion of multiple satellite datasets (MOPITT,AIRS, SCIAMACHY, TES), Atmos. Chem. Phys., 10, 855–876,https://doi.org/10.5194/acp-10-855-2010, 2010.

Kulawik, S. S., J. Worden, A. Eldering, K. Bowman, M. Gunson, G. B. Osterman, L. Zhang, S. A. Clough, M. W. Shephard, and R. Beer (2006), Implementation of cloud 18 retrievals for Tropospheric Emission Spectrometer (TES) atmospheric retrievals: Part 1. Description and characterization of errors on trace gas retrievals, J. Geophys. Res., 111(D24), 2006.

Lelieveld, J., Gromov, S., Pozzer, A., Taraborrelli, D., Global tropospheric hydroxyl distribution, budget and reactivity. Atmos. Chem. Phys. 16, 12477–12493. https:// doi.org/10.5194/acp-16-12477-2016, 2016.

Liu, J., K. W. Bowman, D. S. Schimel, N. C. Parazoo, Z. Jiang, M. Lee, A. A. Bloom, D. Wunch, C. Frankenberg, Y. Sun, C. W. O'Dell, K. R. Gurney, D. Menemenlis, M. Gierach, D. Crisp, and A. Eldering, Contrasting carbon cycle responses of the tropical continents to the 20152016 El Niño, *Science*, *358*(6360), eaam5690, doi:10.1126/science.aam5690, 2017.

Martínez-Alonso, S., Deeter, M., Worden, H., Borsdorff, T., Aben, I., Commane, R., Daube, B., Francis, G., George, M., Landgraf, J., Mao, D., McKain, K., and Wofsy, S.: 1.5 years of TROPOMI CO measurements: comparisons to MOPITT and ATom, Atmos. Meas. Tech., 13, 4841–4864, https://doi.org/10.5194/amt-13-4841-2020, 2020.

Martínez-Alonso, S., Aben, I., Baier, B. C., Borsdorff, T., Deeter, M. N., McKain, K., Sweeney, C., and Worden, H.: Evaluation of MOPITT and TROPOMI carbon monoxide retrievals using AirCore *in situ* vertical profiles, Atmos. Meas. Tech. Discuss. [preprint], https://doi.org/10.5194/amt-2022-54, in review, 2022.

McManus, J. B., Zahniser, M. S., Nelson, D. D., Shorter, J. H., Herndon, S., Wood E., and Wehr, R.: Application of quantum cascade lasers to high-precision atmospheric trace gas measurements, Opt. Eng., 49(11), 111124, doi:10.1117/1.3498782, 2010.

McMillan, W., Barnet, C., Strow, L., Chahine, M. T., McCourt, M. L., Warner, J. X., Novelli, P. C., Korontzi, S., Maddy, E. S., and S. Datta, S: Daily global maps of carbon monoxide from NASA's Atmospheric Infrared Sounder." Geophysical Research Letters 32, no. 11, 2005.

Miyazaki, K., K. Bowman, T. Sekiya, H. Eskes, F. Boersma, H. Worden, N. Livesey, V. H. Payne, K. Sudo, Y. Kanaya, M. Takigawa, and K. Ogochi, Updated tropospheric chemistry reanalysis and emission estimates, TCR-2, for 20052018, *Earth System Science Data*, *12*(3), 22232259, doi:https://doi.org/10.5194/essd-12-2223-2020, 2020.

Moncet, J-L., Uymin, G., Liang, P. and Lipton, A.E: Fast and accurate radiative transfer in the thermal regime by simultaneous optimal spectral sampling over all channels. Journal of the Atmospheric Sciences, vol 72, 2622-2641, doi: 0.1175/JAS-D-14-0190.1, 2015.

Myhre, G., Shindell, D., Breon, F.-M., Collins, W., Fuglestvedt, J., Huang, J., Koch, D., Lamarque, J.-F., Lee, D., Mendoza, B., Nakajima, T., Robock, A., Stephens, G., Takemura, T., Zhang, H., Climate Change 2013: The Physical Science Basis. In: Contribution of Working Group I to the Fifth Assessment Report of the Intergovernmental Panel on Climate Change, chapter Anthropogenic and Natural Radiative Forcing. Cambridge University Press, pp. 659–740, 2014.

Nalli, N.R.; Tan, C.; Warner, J.; Divakarla, M.; Gambacorta, A.; Wilson, M.; Zhu, T.; Wang, T.; Wei, Z.; Pryor, K.; Kalluri, S.; Zhou, L.; Sweeney, C.; Baier, B.C.; McKain, K.; Wunch, D.; Deutscher, N.M.; Hase, F.; Iraci, L.T.; Kivi, R.; Morino, I.; Notholt, J.; Ohyama, H.; Pollard, D.F.; Té, Y.; Velazco, V.A.; Warneke, T.; Sussmann, R.; Rettinger, M. Validation of Carbon Trace Gas Profile Retrievals from the NOAA-Unique Combined Atmospheric Processing System for the Cross-Track Infrared Sounder. *Remote Sens.* **2020**, *12*, 3245. https://doi.org/10.3390/rs12193245.

Qu, Z., Henze, D. K., Worden, H. M., Jiang, Z., Gaubert, B., Theys, N., & Wang, W.: Sector-based top-down estimates of NO_x, SO_2, and CO emissions in East Asia. *Geophysical Research Letters*, 49, e2021GL096009. https://doi.org/10.1029/2021GL096009, 2022.

Reid, J. S., Koppmann, R., Eck, T. F., and Eleuterio, D. P.: A review of biomass burning emissions part II: intensive physical properties of biomass burning particles, Atmos. Chem. Phys., 5, 799–825, https://doi.org/10.5194/acp-5-799-2005, 2005.

Rodgers, C. D.: Inverse Methods for Atmospheric Sounding, Theory and Practice, World Scientific Publishing, London, 2000.

Rodgers, C. D. and Connor, B. J.: Intercomparison of remote sounding instruments, J. Geophys. Res., 108, 4116, doi:10.1029/2002jd002299, 2003.

Santoni, G. W., Daube, B. C., Kort, E. A., Jiménez, R., Park, S., Pittman, J. V., Gottlieb, E., Xiang, B., Zahniser, M. S., Nelson, D. D., McManus, J. B., Peischl, J., Ryerson, T. B., Holloway, J. S., Andrews, A. E., Sweeney, C., Hall, B., Hintsa, E. J., Moore, F. L., Elkins, J. W., Hurst, D. F., Stephens, B. B., Bent, J., and Wofsy, S. C.: Evaluation of the airborne quantum cascade laser spectrometer (QCLS) measurements of the carbon and greenhouse gas suite – CO2, CH4, N2O, and CO – during the CalNex and HIPPO campaigns, Atmos. Meas. Tech., 7, 1509 1526, doi:10.5194/amt-7-1509-2014, 2014.

Seinfeld, J.H. and Pandis, S.N.: Atmospheric Chemistry and Physics. John Wiley and Sons, New York, 1998.

Smith, N., and Barnet, C. D.: CLIMCAPS observing capability for temperature, moisture, and trace gases from AIRS/AMSU and CrIS/ATMS, Atmos. Meas. Tech., 13, 4437-4459, https://doi.org/10.5194/amt-13-4437-2020, 2020.

Strode, S. A., Liu, J., Lait, L., Commane, R., Daube, B., Wofsy, S., Conaty, A., Newman, P., and Prather, M.: Forecasting carbon monoxide on a global scale for the ATom-1 aircraft mission: insights from airborne and satellite observations and modeling, Atmos. Chem. Phys., 18, 10955–10971, https://doi.org/10.5194/acp-18-10955-2018, 2018.

Susskind, J., C. D. Barnet, and J. M. Blaisdell: Retrieval of atmospheric and surface parameters from AIRS/AMSU/HSB data in the presence of clouds, IEEE Trans. Geosci. Remote Sens., 41, 390–409, 2003.

Suto, H., Kataoka, F., Kikuchi, N., Knuteson, R. O., Butz, A., Haun, M., Buijs, H., Shiomi, K., Imai, H., and Kuze, A.: Thermal and near-infrared sensor for carbon observation Fourier transform spectrometer-2 (TANSO-FTS-2) on the Greenhouse gases Observing SATellite-2 (GOSAT-2) during its first year in orbit, Atmos. Meas. Tech., 14, 2013–2039, https://doi.org/10.5194/amt-14-2013-2021, 2021.

Sweeney, C., Karion, A., Wolter, S., Newberger, T., Guenther, D., Higgs, J. A., Andrews, A. A., Lang, P. M., Neff, D. Dlugokencky, et al.: Seasonal climatology of CO2 across North America from aircraft measurements in the NOAA/GML Global Greenhouse Gas Reference Network, J. Geophys. Res. Atmos., 120, 5155–5190, doi:10.1002/2014JD022591, 2015.

Sweeney, C., K. McKain, J. Higgs, S. Wolter, A. Crotwell, D. Neff, E. Dlugokencky, G. Petron, M. Madronich, E. Moglia, M. Crotwell, J. Mund. NOAA Earth System Research Laboratories, Global Monitoring Laboratory. NOAA Carbon Cycle and Greenhouse Gases Group aircraft-based measurements of CO2, CH4, CO, N2O, H2 & SF6 in flask-air samples taken since 1992. http://dx.doi.org/10.7289/V5N58JMF, 2021.

Tang, W., Worden, H. M., Deeter, M. N., Edwards, D. P., Emmons, L. K., Martínez-Alonso, S., Gaubert, B., Buchholz, R. R., Diskin, G. S., Dickerson, R. R., Ren, X., He, H., and Kondo, Y: Assessing Measurements of Pollution in the Troposphere (MOPITT) carbon monoxide retrievals over urban versus non-urban regions, Atmos. Meas. Tech., 13, 1337–1356, https://doi.org/10.5194/amt-13-1337-2020, 2020.

Thompson, C. R., Wofsy, S. C., Prather, M. J., Newman, P. A., Hanisco, T. F., Ryerson, T. B., Fahey, D. W., Apel, E. C., Brock, C. A., Brune, W. H., Froyd, K., Katich, J. M., Nicely, J. M., Peischl, J., Ray, E., Veres, P. R., Wang, S., Allen, H. M., Asher, E., Bian, H., Blake, D., Bourgeois, I., Budney, J., Bui, T. P., Butler, A., Campuzano-Jost, P., Chang, C., Chin, M., Commane, R., Correa, G., Crounse, J. D., Daube, B., Dibb, J. E., DiGangi, J. P., Diskin, G. S., Dollner, M., Elkins, J. W., Fiore, A. M., Flynn, C. M., Guo, H., Hall, S. R., Hannun, R. A., Hills, A., Hintsa, E. J., Hodzic, A., Hornbrook, R. S., Huey, L. G., Jimenez, J. L., Keeling, R. F., Kim, M. J., Kupc, A., Lacey, F., Lait, L. R., Lamarque, J., Liu, J., McKain, K., Meinardi, S., Miller, D. O., Montzka, S. A., Moore, F. L., Morgan, E. J., Murphy, D. M., Murray, L. T., Nault, B. A., Neuman, J. A., Nguyen, L., Gonzalez, Y., Rollins, A., Rosenlof, K., Sargent, M., Schill, G., Schwarz, J. P., Clair, J. M. S., Steenrod, S. D., Stephens, B. B., Strahan, S. E., Strode, S. A., Sweeney, C., Thames, A. B., Ullmann, K., Wagner, N., Weber, R., Weinzierl, B., Wennberg, P. O., Williamson, C. J., Wolfe, G. M., & Zeng, L.: The NASA Atmospheric Tomography (ATom) Mission: Imaging the Chemistry of the Global Atmosphere, *Bulletin of the American Meteorological Society*, *103*(3), E761-E790. https://journals.ametsoc.org/view/journals/bams/103/3/BAMS-D-20-0315.1.xml, 2022

Wofsy, S. C., Afshar, S., Allen, H. M., Apel, E. C., Asher, E. C., Barletta, B., Bent, J., Bian, H., Biggs, B. C., Blake, D. R., Blake, N., Bourgeois, I., Brock, C. A., Brune, W. H., Budney, J. W., Bui, T. P., Butler, A., Campuzano-Jost, P., Chang, C. S., Chin, M., Commane, R., Correa, G., Crounse, J. D., Cullis, P. D., Daube, B. C., Day, D. A., Dean-Day, J. M., Dibb, J. E., DiGangi, J. P., Diskin, G. S., Dollner, M., Elkins, J. W., Erdesz, F., Fiore, A. M., Flynn, C. M., Froyd, K. D., Gesler, D. W., Hall, S. R., Hanisco, T. F., Hannun, R. A., Hills, A. J., Hintsa, E. J., Hoffman, A., Hornbrook, R. S., Huey, L. G., Hughes, S., Jimenez, J. L., John- son, B. J., Katich, J. M., Keeling, R. F., Kim, M. J., Kupc, A., Lait, L. R., Lamarque, J.-F., Liu, J., McKain, K., Mclaughlin, R. J., Meinardi, S., Miller, D. O., Montzka, S. A., Moore, F. L., Morgan, E. J., Murphy, D. M., Murray, L. T., Nault, B. A., Neu- man, J. A., Newman, P. A., Nicely, J. M., Pan, X., Paplawsky, W., Peischl, J., Prather, M. J., Price, D. J., Ray, E., Reeves, J. M., Richardson, M., Rollins, A. W., Rosenlof, K. H., Ryerson, T. B., Scheuer, E., Schill, G. P., Schroder, J. C., Schwarz, J. P., St. Clair, J. M., Steenrod, S. D., Stephens, B. B., Strode, S. A., Sweeney, C., Tanner, D., Teng, A. P., Thames, A. B., Thompson, C. R., Ullmann, K., Veres, P. R., Vieznor, N., Wag- ner, N. L., Watt, A., Weber, R., Weinzierl, B., Wennberg, P. O., Williamson, C. J., Wilson, J. C., Wolfe, G. M., Woods, C. T., and Zeng, L. H.: ATom: Merged Atmospheric Chemistry, Trace Gases, and Aerosols, ORNL DAAC [data set], Oak Ridge, TN, USA, https://doi.org/10.3334/ORNLDAAC/1581, 2018.

Worden, H. M., J. Logan, J. R. Worden, R. Beer, K. Bowman, S. A. Clough, A. Eldering, B. Fisher, M. R. Gunson, R. L. Herman, S. S. Kulawik, M. C. Lampel, M. Luo, I. A. Megretskaia, G. B. Osterman, M. W. Shephard, Comparisons of Tropospheric Emission Spectrometer (TES) ozone profiles to ozonesodes: methods and initial results, *J. Geophys. Res., 112, D03309*, doi:10.1029/2006JD007258 , 2007.

Worden, H. M., Deeter, M. N., Frankenberg, C., George, M., Nichitiu, F., Worden, J., Aben, I., Bowman, K. W., Clerbaux, C., Coheur, P. F., de Laat, A. T. J., Detweiler, R., Drummond,J. R., Edwards, D. P., Gille, J. C., Hurtmans, D., Luo, M., Martínez-Alonso, S., Massie, S., Pfister, G., and Warner, J. X.: Decadal record of satellite carbon monoxide observations, Atmos. Chem. Phys., 13, 837–850, https://doi.org/10.5194/acp-13-837-2013, 2013.

Zheng, B., Chevallier, F., Yin, Y., Ciais, P., Fortems-Cheiney, A., Deeter, M. N., Parker, R. J., Wang, Y., Worden, H. M., and Zhao Y. : Global atmospheric carbon monoxide budget 2000–2017 inferred from multi-species atmospheric inversions: Earth Syst. Sci. Data, 11, 1411–1436, doi.org/10.5194/essd-11-1411-2019, 2019.